Graphene Based Luminescence and Optoelectronics

By

Irfan Ahmed Choudhury (122403)
Fahad Al Mamun (122443)

A Thesis Submitted to the Academic Faculty in Partial Fulfillment of the Requirements for the Degree of

BACHELOR OF SCIENCE IN ELECTRICAL AND ELECTRONIC ENGINEERING

Department of Electrical and Electronic Engineering

Islamic University of Technology (IUT)

Gazipur, Bangladesh

November 2016

CERTIFICATE OF RESEARCH

This is to certify that the work presented in this thesis paper is the outcome of research carried out by the candidate under the supervision of Dr. Syed Iftekhar Ali, Associate Professor, Electrical and Electronic Engineering (EEE). It is also declared that neither this thesis paper nor any part thereof has been submitted anywhere else for the reward of any degree or any judgment.

Authors

Fahad Al Mamun

Irfan Ahmed Choudhury

Signature of Supervisor

Dr. Syed Iftekhar Ali
AssociateProfessor
Electrical and Electronic Engineeringg (EEE)
Islamic University of Technology (IUT)

Signature of Head of the Department

Prof. Dr. Md. Ashraful Hoque
Head of the Department
Electrical and Electronic Engineering (EEE)
Islamic University of Technology (IUT)

Table of Contents

List of Figures

List of Acronyms

PEDOT	Poly 3,4-ethlene-dioxythiophene
PSS	Poly styrene sulfonate
ITO	Indium tin oxide
PCE	Power Conversion Efficiency
CVD	Chemical Vapor Deposition
PMMA	Polymethyl Methacrylate
DI	Deionized
PVD	Physics Vapor Deposition
GQD	Graphene Quantum Dots
EQE	External Quantum Efficiency
FWHM	Full Width at Half Maximum
CNMR	Carbon-13 Nuclear Magnetic Resonance
TEM	Transmission Electron Microscopy
TPBI	1,3,5-tris(N-phenylbenzimidizol-2-yl)benzene
TCTA	Tris(4-carbazoyl-9-ylphenyl)amine
SOHIL	A self-organized polymeric hole injection layer
EML	Emitting Layer
HOMO	Highest Occupied Molecular Orbital
LUMO	Lowest Unoccupied Molecular Orbital

ACKNOWLEDGMENTS

We express our gratitude and indebtedness to our superviser Dr.Syed Iftekhar Ali, Associate Professor,Department of EEE,IUT for providing precious guidance, inspiring discussions and constant supervision throughout the course of this work. His help, constructive criticism, and conscientious efforts made it possible to present the work. It's our goodness that in spite of having a tight and busy schedule our supervisor has found time to help and guide us. For this, we again express our greatness to him. We are also grateful to EEE Department of IUT for providing us the opportunity to present this work.

Abstract

Charge carriers in graphene mimic two-dimensional massless Dirac fermions with linear energy dispersion, resulting in unique optical and electronic properties. They exhibit high mobility and strong interaction with electromagnetic radiation over a broad frequency range. Interband transitions in graphene give rise to pronounced optical absorption in the mid-infrared to visible spectral range. Free-carrier intraband transitions, on the other hand, cause low frequency absorption, which varies significantly with charge density and results in strong light extinction at high carrier density. These properties together suggest a rich variety of possible optoelectronic applications for graphene. But graphene is a zero bandgap material which hinders the uses of graphene in luminescent application.

In this thesis paper, we have addressed this bandgap problem and reviewed some of the important achievements so far in introducing bandgap in graphene.we have also investigated the optoelectronic properties of graphene and reviewed some of the significant applications.Later, we have discussed about graphene quantum dot and their applications in multicolor light emitting applications and in solar cells.

Chapter 1

Introduction

1.1 Background

Graphene is a material in a two-dimensional single atomic layer and made of carbon atoms bonded in a honeycomb lattice (shown in Figure 1.1). Graphene is the basic structure of graphite, carbon nanotubes, fullerenes and diamond (shown in Figure 1.2). Since its discovery by scientists Andre Geim and Kostya Novoselov in 2004, it is predicted that graphene will bring a new revolution to the current carbon-based electronics on account of its remarkable physical properties. Graphene is the strongest (stronger than diamond) and thinnest (thinner than a paper) material that has ever been known. In addition, graphene is much more flexible than silicon, which is the most widely used material in the electronic world. And it was reported that graphene could be stretched by 20% while silicon could only be stretched by 1% [1]. Moreover, it has been observed that graphene conducts heat and electricity with great efficiency. Additionally, graphene will provide scientists an excellent model to study relativistic quantum phenomena [2, 3] such as the quantum Hall effect [4] in condensed matter material.

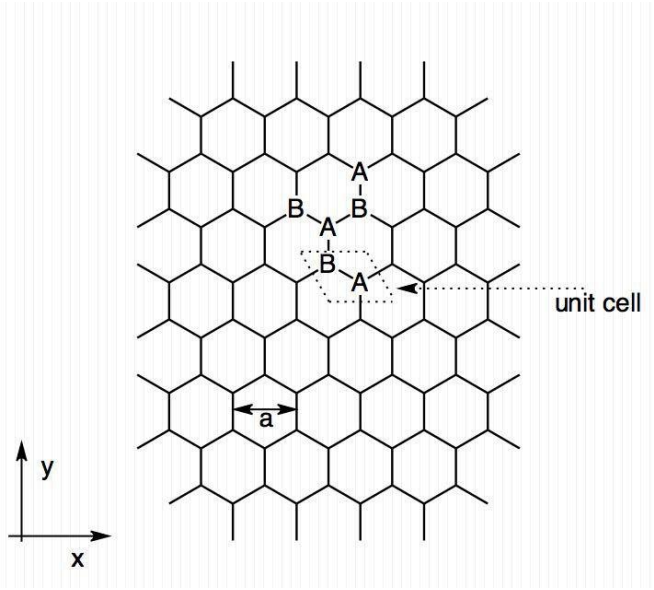

Figure 1.1. The hexagonal honeycomb lattice of graphene with the primitive vector a = 2.46 Å. The unit cell consists of two sublattices: A and B.

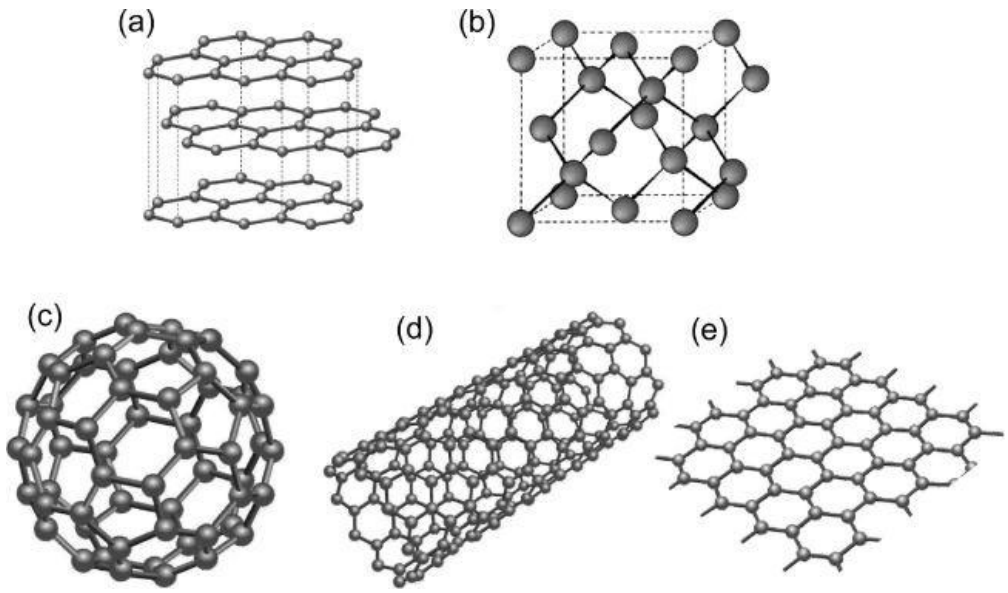

Figure 1.2. (a) Graphite: stack of graphene sheets; (b) Diamond: cubic; (c) Fullerenes: closed cage of carbon; (d) Carbon nanotube: rolled-up sheets of graphene; (e) Graphene. From Ref. [5]

1.2 Structure of Graphene

In graphene, there are two carbon atoms per unit cell, displayed as A and B in Figure 1.1. Each carbon atom, which is the sixth element (of periodic table) with a total of 6 electrons, has the electron configuration of $1s^2 2s^2 2p^2$. Here one 2s orbital per carbon in graphene is combined with the $2p_x$ and $2p_y$ to form three sp2 orbitals. And the sp2 orbital of each carbon is then bonded with the adjacent sp2 orbitalforming a strong covalent σ band that is 1.42 Å long. The remaining 2pz orbital, which is perpendicular to the planar structure, forms a covalent π band with the neighboring carbon atom.

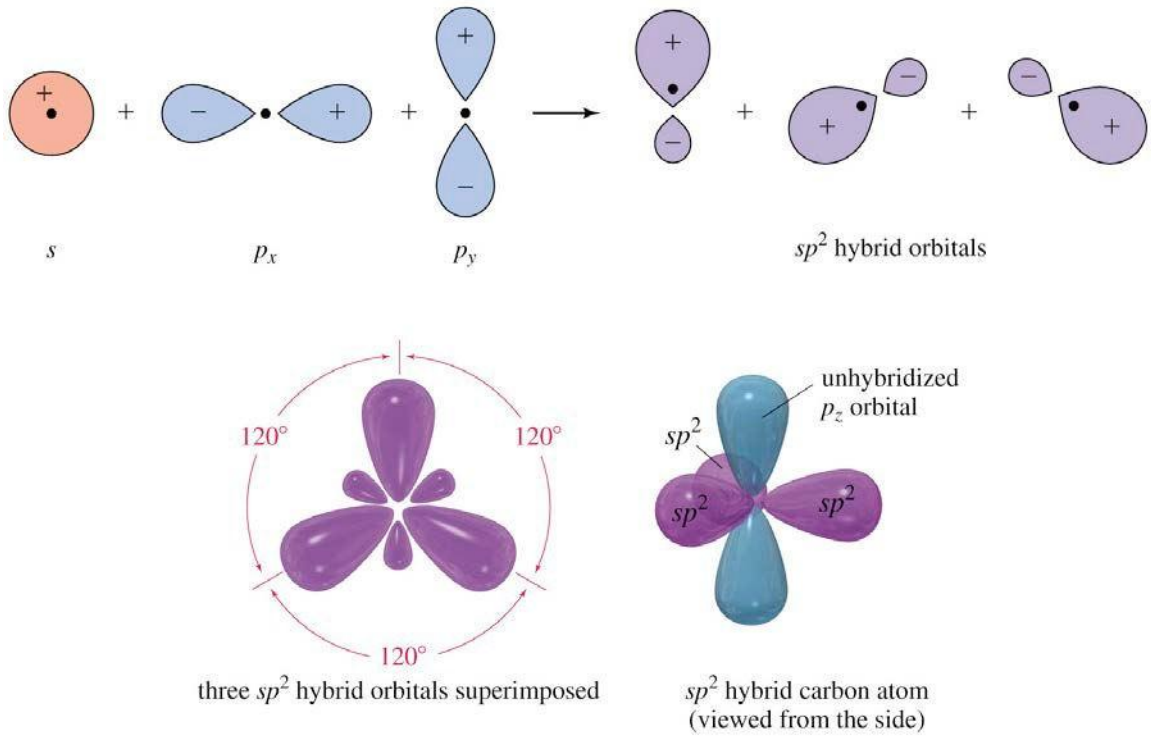

Figure 1.3. The bonding process of graphene structure: one 2s orbital is combined with the $2p_x$ and $2p_y$ to form three sp2 orbitals, and the remaining $2p_z$ orbital is perpendicular to the planar structure.From Ref. [6]

In addition, the π band is half-filled, and it is responsible for the conductivity of graphene with an extra electron from each p orbital. The bonding process of graphene structure is illustrated in Figure 1.3. The σ and π bands in graphene form the Fermi surface, which is characterized as six double cones as shown in Figure 1.4. And in the undoped environment, the corners (depicted as two Fermi points: K and K', and they are also displayed on the first Brillouin zone of graphene in Figure 1.5) of these six double cones are the Fermi level of graphene, and are separating conduction and valence bands. According to this band structure, graphene is a zero gap semiconductor. On the other hand, it means that the density state of the intrinsic graphene is zero at the Fermi level.

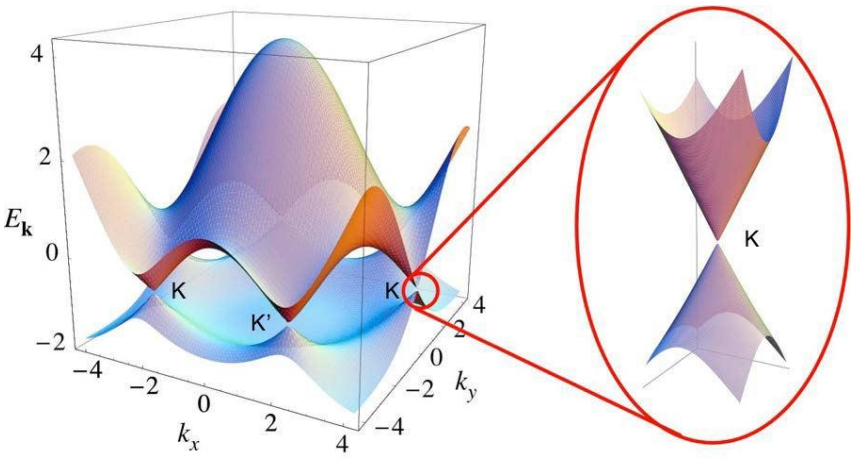

Figure 1.4. Band structure of graphene. There are six Dirac points, but only two of them are non-equivalent, and they are denoted as K and K'. The conduction and valence band are touching at the Dirac points. From Ref. [7].

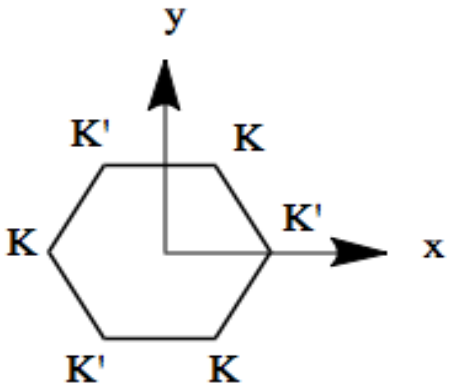

Figure 1.5. The first Brillouin zone of graphene with two non-equivalent Dirac points denoted as K and K'. The points K and K' are the touching points of the Energy bands.

Chapter 2

Optical Transition in Graphene

The optical response of graphene can be divided into two fundamental processes: inter-band and intra-band optical transitions [8, 9–11]. Inter-band transitions dominate the absorption channel in the mid-/near-infrared and visible spectral range. The corresponding graphene sheet conductivity for photons that leads to excitations of the graphene band structure in the region of linear dispersion is given by the frequency-independent universal constant of $\pi e^2/2h$ [12, 13]. Whereas the inter-band transitions have been extensively characterized, the influence of intra-band transitions, i.e. of the free carrier absorption, on the transient optical response of graphene in the visible is yet to be established. At longer probe wavelengths, the influence of intra-band transitions becomes stronger, and the role of these transitions in the transient response of photoexcited graphene in the mid-infrared and THz spectral range has recently been reported [14, 15]. A full understanding of this dynamical response is important for applications of graphene in ultrafast photonic devices, as in saturable absorbers. As depicted in Fig. 2(a). Intra-band transitions require change in *k* thus phonon mediation; therefore, their properties are closely related to the electrical transport properties of graphene. These optical transitions are dominating at low photon energies, i.e. the far-IR. In contrast, inter-band transitions dominate at near-IR and visible frequencies.

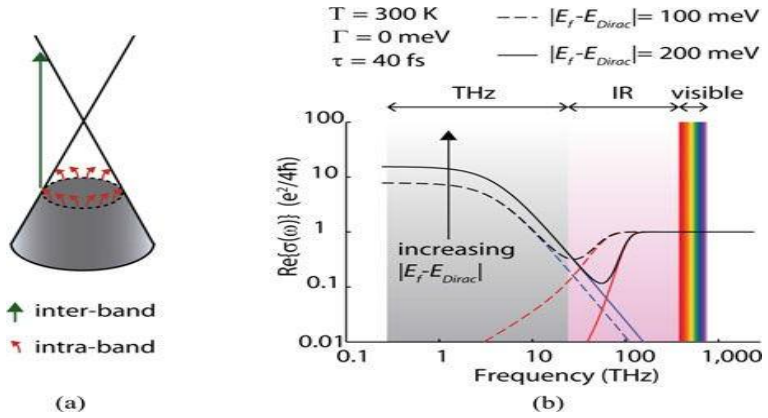

Fig.2.1 (a) Optical transitions in graphene. (b) Optical conductivity versus frequency for two different Fermi levels (extracted from Ref. [9]). Contribution due to intra/inter-band transitions are shown in blue/red, respectively.

However, as can be noticed in Fig. (b) and information from[16-18], in the mid-IR to terahertz ranges, there is a very strong dependence of optical conductivity with Fermi level. Therefore, the optical conductivity of graphene can be effectively modified by electro-statically controlling its Fermi level. This tunability enables the realization of graphene-based reconfigurable opto-electronic devices [11], [19] such as ultra-fast electro-absorption infrared modulators, phase shifters, beam steerers, and so on. In the far-IR and terahertz ranges, as Fermi level becomes closer to Dirac point, the density of states available for intra-band transitions decreases thus its optical conductivity reduces. Here, as frequency increases, the magnitude of its optical conductivity exhibits a Drude roll-off. At mid-IR frequencies, both intra-band and inter-band transitions become significant and these trends might no longer hold.

Chapter 3

Bandgap Engineering

3.1 Bandgap Dilemma

Graphene is currently regarded as one of the most promising materialswith the characteristics of a single atomic layer and high electron mobility, for use in the next generation of high-speed nanodevices [20−21] However, pristine graphene has no bandgap at the Fermi level (E_f) at the K point, which means that the highest occupied and lowest unoccupied states coincide at this K point. The dispersion of the two corresponding energy bands is approximately linear near the K point and differ in that respect from the parabolic dispersions close to the valence band maximum (E_{VBM}) and the conduction band minimum (E_{CBM}) of a semiconductor.

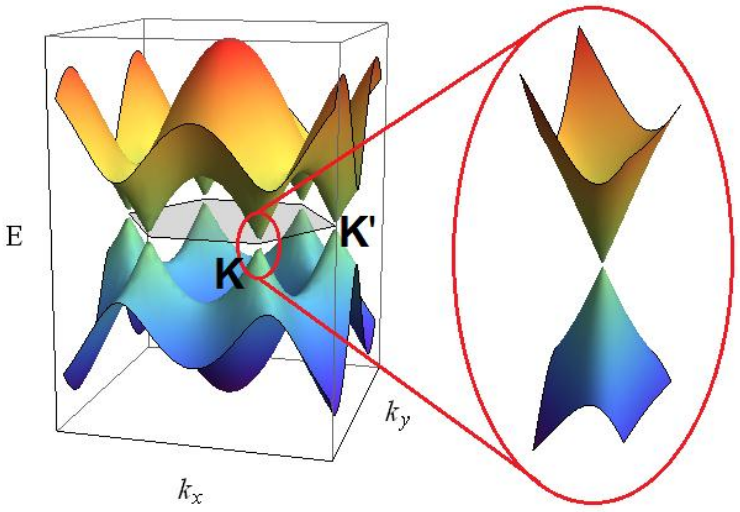

Figure3.1: E-K diagram of pristine graphene

Several schemes, therefore, have been adopted to form a band gap in graphene by, for example, hole or molecular doping[5, 6], electron confinement with quasi one dimensional graphene nanoribbons[7, 8], a gate voltage applied perpendicularly to bilayer graphene[9], and chemical functionalization by adsorbing external atoms or molecules on SLG[22, 23]. The opening of a band gap by functionalizing graphene with atoms and

molecules, in particular, has been utilized efficiently to induce symmetry-breaking in the charge distribution between the A and B carbon sublattices of a hexagonal unit cell of SLG [24-25]. The degradation of the unique Dirac nature of graphene by adsorbates, however, appears to be a serious drawback for industrial applications and needs to be tackled.

This gapless semimetallic nature of graphene, however, needs to be converted into a semiconducting phase with a finite band gap (Eg) to control the conductivity in most electronic applications [26-30] Because the massless Dirac fermions in graphene showing ballistic charge transport [31-33], even at room temperature [34], are ideal charge carriers for fast circuit devices, research efforts have been continued to open a tunable band gap in graphene. To this end, there have been continuous efforts to realize the band gap in graphene.

3.2 Recent Bandgap Opening Methods

In this section recent methods for opening bandgap in graphene are reviewed.

3.2.1 Using Na^+ ions

Sung etal. reported a new route to open a band gap (Eg) at DP in a controlled way by depositing positively charged Na +ions on single layer graphene formed on 6H-SiC((0001surface [35]. The doping of low energy Na +ions is found to deplete the π^* band of graphene above the DP, and simultaneously shift the DP downward away from Fermi energy indicating the opening of Eg. The band gap increases with increasing N +acoverage with a maximum Egalmost equal to 0.70 eV. Thecore-level data, C 1s, Na 2p, and Si 2p, consistently suggest that Na +ions do not intercalate through graphene, but produce a significant charge asymmetry among the carbon atoms of graphene to cause the opening of a band gap.

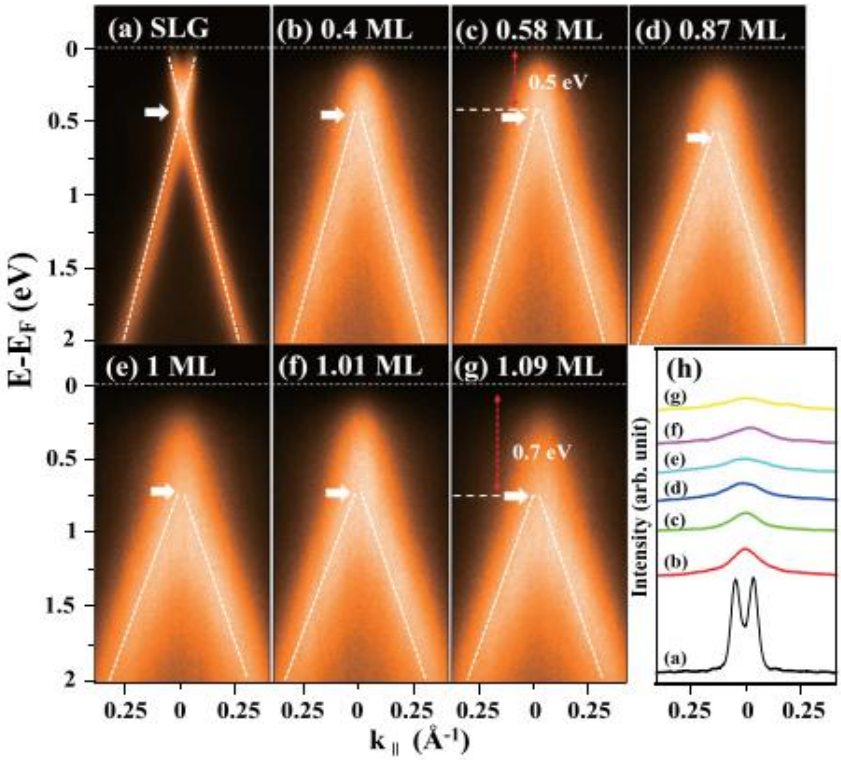

Figure3.2:Changes in the p-band of SLG near the K-point as a function of Na $^{+}$coverage; the clean SLG (a) shows a sharp p-band, which broadens and shift sdown with increasing Na $^{+}$ coverage [(b)–(g)]. The MDC of the band at Fermi level (h)[35]

In this paper [35] the authors reported another route to engineer the band gap of graphene by doping low energy N +aions on a single layer graphene (SLG) formed on 6H-SiC (0001surface)changes in the π -band of graphene and in the core levels (C 1s,Na2p, and Si 2p) induced by the doped Na +ions by utilizing angle-resolved photoemission spectroscopy (ARPES) and high-resolution core level spectroscopy (HRCLS) with synchrotron photons.

The charge asymmetry among carbon atoms caused by the Na $^{+}$ions is found to be much more significant than that by neutral Na atoms for the two graphene sublattices as reported for Na on Ir [36] superlattice produced a maximum band gap greater than 0.70 eV at DP. The size of the band gap can rather easily be controlled by varying ion coverage. Interestingly, despite the large band gap produced, the novel electronic properties of graphene due to its Dirac fermions such as the linear nature of the p-band and the mobility appear to remain almost intact with the doping of Na +ions. Interestingly the bonding of Na +ions on graphene is found to be weaker than that of neutral hydrogen or nitrogen atoms doped from energized sources [37-39] since the clean graphene is restored by flashing the Na-+doped graphene at a temperature lower than the desorption temperature of such hydrogen or nitrogen. Therefore, the doping of Na +ions on SLG turns out to be an efficient way to form a tunable band gap on graphene without deteriorating its novel electrical properties [40].

3.2.2 Using slow Cs^+ ions:

A new method reported containg wide band gap engineering for graphene using slow Cs+ ions, which allows both fine-tuning and on–off switching capability of the band gap in a range suitable for most applications without modifying or deteriorating the relativistic nature of the Dirac fermions[41]. The doping of Cs $^+$ions opens the band gap up to Eg0.68= eV, which can be closed completely by adding neutral Cs atoms, as observed in ARPES.

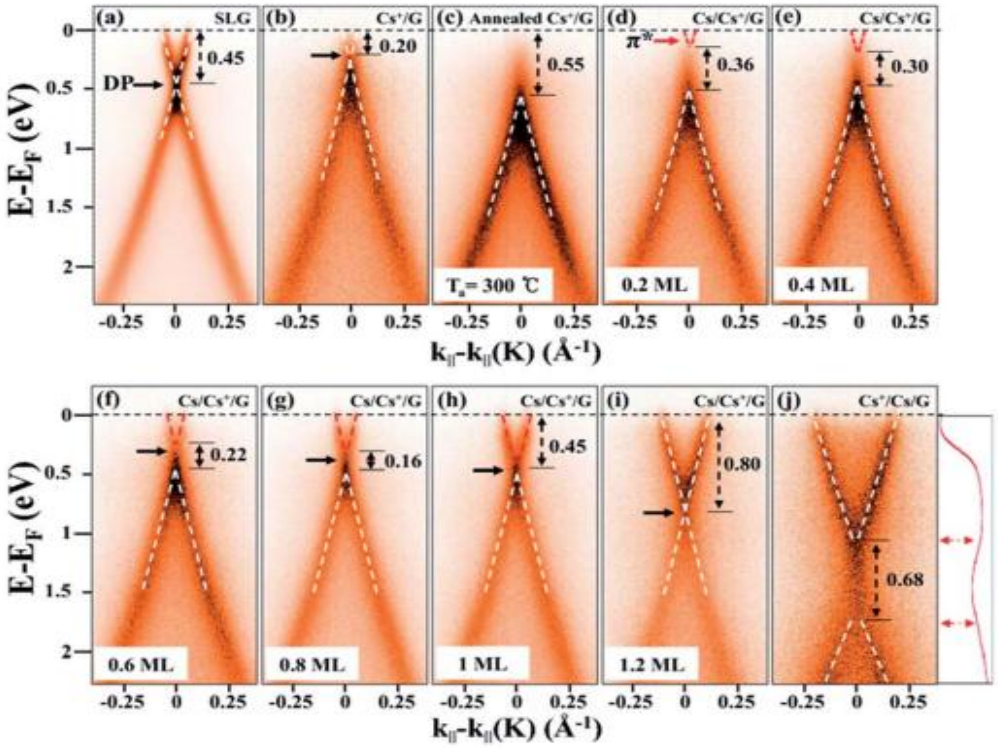

Figure3.3 : Opening and fine-tuning a band gap in the p-band of graphene) a) SLG, (b) Cs^+ions doped (1.0 ML) graphene ($Cs/^+G$), (c) $Cs/^+G$ annealed at ^{o}300C, (d)–(i)Cs added $Cs/^+G$ ($Cs/Cs/^+G$) with increasing Cs, and (j) Cs^+iondeposited on Cs pre-adsorbed graphene ($Cs/^+Cs/G$).[41]

The figure above shows the changes in the linear π-band of SLG upon surface treatments with Cs^+ions or neutral Cs atoms obtained from (a) SLG, (b) 1.0 monolayer (ML) Cs^+ions doped graphene)$Cs/^+G$), (c) $Cs/^+G$ annealed at 300℃, (d)–(i) Cs added $Cs/^+G$) $Cs/Cs/^+G$) with increasing Cs coverage θCs, and (j) Cs^+Ion deposited on Cs pre-adsorbed graphene ($Cs/^+Cs/G$). These bands were obtained along the direction perpendicular to theΓ →K direction with the center at the K-point. The bands to locate the top (bottom) of the π-(π *) band are depicted as white dashed lines in Fig. 1, drawn by determining the slopes of the bands from the neighboring momentum distribution curves (MDCs) obtained at two different energies near the Dirac point (DP).

3.2.3 BN co-doped grapheme

Bo-Yao wang et al. demonstrated a nonlinear behavior for the bandgap opening of doped graphene by controlling the concentration of B and N co-dopants[42]. X-ray absorption and emission spectra reveal that the bandgap increases from 0 to 0.6 eV as the concentration of BN dopants is increased from 0 to 6% while the bandgap closes when the doping concentration becomes 56%This nonlinear behavior of bandgap opening of the BN-doped graphene depending on the BN concentrations is consistent with the valence band photoemission spectroscopic measurements. The spatially resolved B, N and CK-edge scanning transmission x-ray microscopy and their x-ray absorption near-edge structure spectra all support the scenario of the development of h-BN-like domains at high concentrations of BN This study revealed truely a new way to engineer the bandgap of low-dimensional systems.

Engineering doping [43] which is a well-known method for modulating the electronic properties of graphene. Among various boron-nitrides, hexagonal boron-nitride (h-BN) is an effective dopant for inducing a bandgap in graphene [44-53] because it has not only a wide bandgap (with an energy gap range from 3.6 to 7.1 eV)[54,55] also has a similar honeycomb lattice to that of graphene. Doping with B and N atoms may induce a slight shift of E_f, although these atoms have opposite charge-transfer effects (p- and n-type doping) thus[55] providing the potential advantage of a low required gate voltage to give graphene an insulating property. UV-visible light [[14and preliminary bandgap measurements [[15have been performed to reveal the existence of a bandgap in the BN-co-doped graphene at particular doping concentrations.

Despite many research works in this field [44-53]the mechanism of the opening of the bandgap and its correlation with the characters of BN dopant are not yet fully understood. Unsurprisingly, introducing BN dopant breaks the sublattice symmetry, and deviation from the gapless character of graphene is then expected [53].

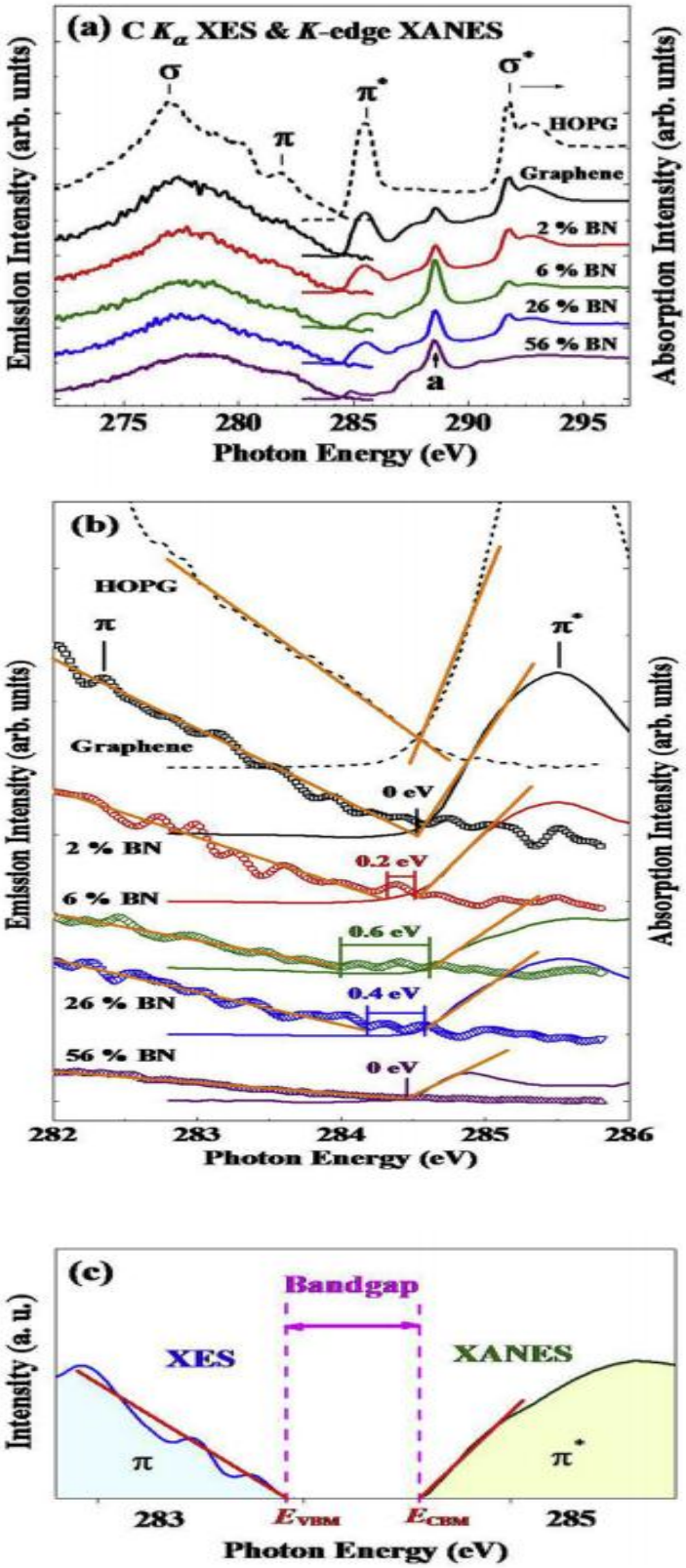

Figure3.4: (a)Normalized C KαXES and K-edge XANES spectra of BNco -doped graphene with various BN concentrations, pristine graphene and HOPG. (b) Magnified*π -π regions of spectra. (c) Scheme of bandgap obtained from the energy between EVBM (valence band maximum) and ECBM (conduction band minimum) [42]

According to previous theoretical studies, the bandgap of graphene is generated by either a local charge density and potential redistribution effect of small BN crystallites or a local quantum confinement effect associated with large h-BN domains. In this study, the bandgap opening of BN-doped grapheme depending on the doping concentrations is obtained by the electronics structure studies experimentally and theoretically. Surprisingly, the bandgap opening is found to be a nonlinear function of the total concentration of BN dopants. Initially, the bandgap increases from 0 to 0.6 eV as the concentration of BN dopants increases from 0 to %6; it then decreases and approaches zero when the BN concentration is increased further to 56%.

3.2.4 Forming Heterojunctions

Cao and co-workers reported about heterojunctions of graphene and other two-dimensional carbonitride materials with natural holes in their monolayers, namely, nitrogenated holey graphene (NHG), g-C3N4, and g-CN, to destroy graphene's sublattice symmetry[56].The heterojunctions, except for that with g-CN, have a direct band gap and that their important band edge states are dominated mainly by their graphene layer. The electric field can open band gaps and reduce the effective mass of electron and hole. The graphene/NHG has a large band gap (186.6 meV) and electron effective mass, which can be reduced from 1.31 to0.014 m 0by applying an electric field of 0.4 V/Å. The NHG/graphene/NHG has the largest band gap of 250.7 meV among all of the graphene-based heterojunctions. The band gap of g-C 3N/4graphene/g-C3N4 can be enlarged from 76.8 to 85.5 meV by applying a perpendicular electricfield (0.6 V/Å). Interestingly, the external electricfield can also convert the indirect band gap of graphene/g-CN into a direct one of 83.3meV. Our results are useful for fast graphene-based nano-optoelectronic devices.

As an alternative way, the graphene-based heterojunctions formed with other 2D materials, such as BN (57,59) and g-C3N4 provide a new method for opening graphene's bandgap. , Mahmood et al. successfully synthesized nitrogenated holey graphene (NHG)[60] new 2D material, with a substantial direct band gap of 1.96 eV[61]. Since one primitive cell of NHG consists of 6 nitrogen and 12 carbon atoms, the NHG is also called C2N. The NHG, a 2D semiconductor with a lattice constant matching that of graphene, can be a potential substitute of the other 2D materials, such as BN and g-C3N4, to form a heterojunction with graphene. It has been known that, if applying an electric field perpendicular to a heterojunction, the interlayer distance and

geometric structure of its layers can be altered, and consequently, the band gap and carrier mobility will be modified. Attempts have been made to enlarge the band gap of grapheme/g-C3N4 with an electric field, and the band gap increases by about one-half when electric field is added to 0.6 V/Å.

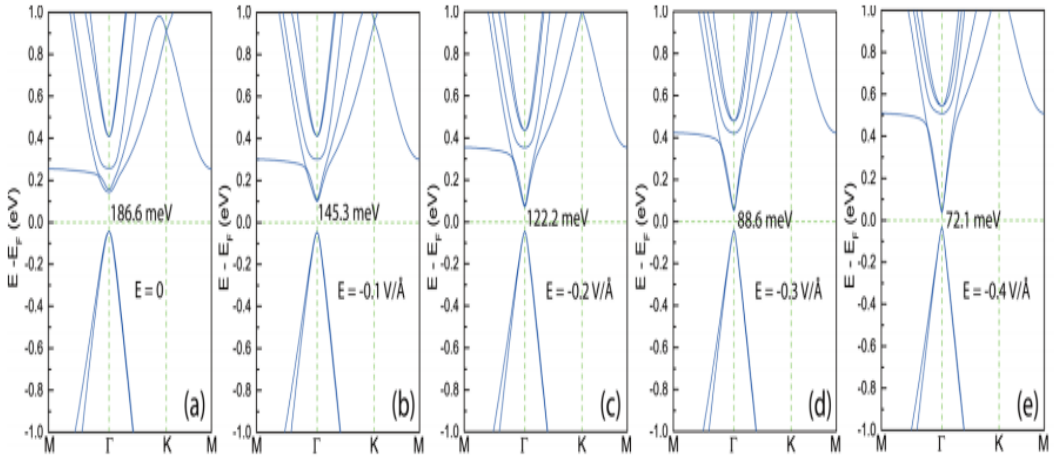

Figure3.5: Band structure of graphene/NHG heterojunction with an electric field of (a) 0 V/Å, (b)−0.1 V/Å, (c)−0.2 V/Å, (d)−0.3 V/Å, and (e) 0.4−V/Å[56]

This fact indicates that the electric field has a remarkable influence on the band gap. With this feature, we can make a trade-off between the band gap and the carrier mobility. By changing the electric field, we can easily increase the band gap with only a slight sacrifice of the carrier mobility,and vice versa. By stacking different 2D monolayers together and applying an electric field, we can obtain various heterojunctions and effectively modify their electronic structures to have a suitable band gap and carrier effective mass, which is very promising for fast graphene-based Optoelectronic nanodevices. Considering that 2D carbonitrides, such as NHG, g-C3N 4, and g-CN, have natural holes in their monolayers, we thus build several heterojunctions of graphene and these 2D carbonitrides. The band gap of graphene can be expected to open because its sublattice symmetry is broken owing to the holes of those carbonitrides. We investigate the electronic structures of graphene/NHG, NHG/graphene/NHG, g-C3N 4 /graphene/gC3N4, and graphene/g-CN heterojunctions because they can be expected to destroy the sublattice symmetry of graphene more remarkably than other combinations, such as graphene/NHG/ graphene and NHG/graphene/graphene.Calculations show that graphene/NHG, NHG/graphene/NHG, and gC3N/4graphene/g-C3N4have a direct band gap and their band edges are mainly determined by their graphene layer. The band gap of graphene can be opened up to 250.7 meV by forming a NHG/graphene/NHG heterojunction. The electron effective mass in graphene/NHG can be reduced from 1.31 to 0.014m $_0$ at an electricfield of

E= 0.4 V/Å. The band gap of g-C3N /4graphene/g-C3N 4can be enlarged from 76.8 to 85.5 meV at E= 0.6 V/Å.

3.2.5 Using slow Li +ions

Ryu and co-workers investigated on the ion-induced modification of the electronic properties of single-layer grapheme (SLG)grown on a SiC((0001 substrate by doping low-energy (5eV) Li +ions [62].They found the opening of a sizable and tunable band gap up to 0.85 eV, which depends on the Li + ion dose as well as the following thermal treatment, and is the largest band gap in the π-band of SLG by any means reported so far. Li 1s core-level data together with the valence band suggest that Li +ions do not intercalate below the topmost graphene layer, but cause a significant charge asymmetry between the carbon sublattices of SLG to drive the opening of the band gap. This experimentprovided a route to producing a tunable graphene band gap by doping Li +ions, which may play a pivotal role in the utilization of graphene in future graphene-based electronic nano devices.

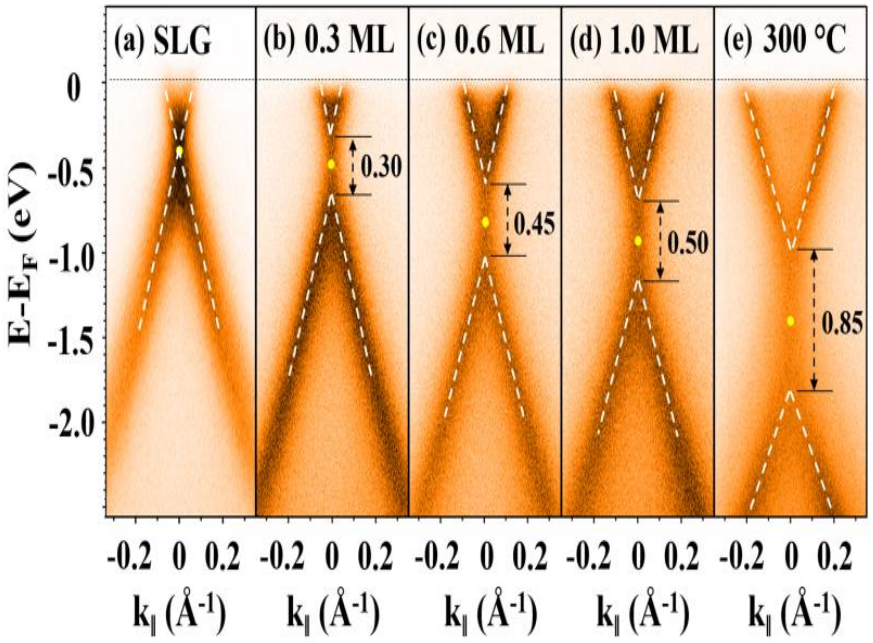

Figure3.6: Changes of the π-band induced by Li^{+}ions as a function of θ and thermal annealing. The π-band obtained from(a)SLG and(b),)c),(d)after doping Li $^{+}$ions of θ=0.3 ML, 0.6 ML, 1.0 ML, and(e)the annealed band in(d)at °300C, respectively[62]

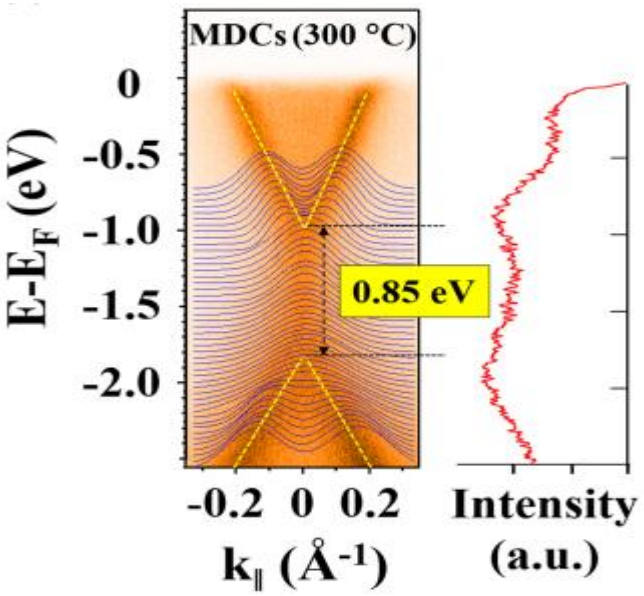

Figure:3.7 MDC(blue curves) and EDC(red curve)around the K-point of the band[62]

.Ryu etalreported that the doping of Li +ions on SLG does indeed open a band gap whose size can be adjusted artificially in proportion to the Li +ion coverage (θ) followed by an annealing procedure up to Eg=0.85 eV. It can be noticed that a minimal adverse effects on the Dirac nature of the π-band by doping Li +ions on SLG. The photoemission data (valence and core levels) suggests that the opening of a band gap by Li +ions is driven essentially by the Li- +induced broken symmetry in the charge distribution among carbon atoms. This way of opening a band gap by doping low-energy Li +ions thus turns out to be quite an effective route for forming a tunable band gap, without damaging the Dirac nature of SLG. sIt wafound that the Li +ions doped on SLG at 90 K are not intercalated but cause a significant charge asymmetry between the two carbon sublattices to open a band gap at the K-point of the Brillouin zone. We further observe that the size of the band gap can be artificially adjusted by controlling the ion coverage, followed by proper thermal annealing. The band gap Eg =0.85 eV thus obtained upon annealing at Ta=°300C from the Li- +doped SLG with θ =1.0 ML turns out to be the largest band gap reported so far from all functionalized SLG samples, using various kinds of atoms or ions. Furthermore, the band gap thus prepared is found to have the lowest in-gap intensity and is also found to preserve the noble nature of the linear π-band, which is quite distinct from other functionalized SLG samples. Thisis the largest bandgap in the π-band of SLG by any means reported so far.

Chapter 4

Production Methods

For the tremendous application of graphene in nanoelectronics and optoelectronics, it is essential to fabricate high-quality graphene in large production. There are different methods of generating graphene. This review summarizes the exfoliation of graphene by mechanical, chemical and thermal reduction and chemical vapor deposition and mentions their advantages and disadvantages. This article also indicates recent advances in controllable synthesis of graphene, illuminates the problems, and prospects the future development in this field.

4.1 Synthesis of Graphene

Synthesis of graphene refers to any process for fabricating or extracting graphene, depending on the desired size, purity and efflorescence of the specific product. In the earlier stage various techniques had been found for producing thin graphitic films. Late 1970's carbon precipitated in the form of thin graphitic layers on transition metal surfaces [63,64]. In 1975, few-layer graphite was synthesized on a single crystal platinum surface via chemical decomposition methods, but was not designated as graphene due to a lack of characterization techniques or per- haps due to its limited possible applications [65].

In those periods, their electronic properties never were investigated because of the difficulty in isolating and transferring them onto insulating substrates. But in the late 90's Ruoff and co-workers tried to isolate thin graphitic flakes on SiO_2 substrates by mechanical rubbing of pat- terned islands on HOPG (Highly Oriented Pyrolytic Graphite) [66]. However there was no report on their electrical property characterization. Using a similar method this was later achieved in 2005 by Kim and co-workers and the electrical properties were reported [67]. But the real prompt advancement in graphene research began after Geim and co-workers first published their work of isolating graphene on to SiO_2 substrate and measuring its electrical properties. After discovery of graphene in 2004 various techniques were developed to produce thin graphitic films and few layer graphene. The experimental evidence of 2D crystals came in 2004 [68] and 2005 [69] when thin flakes of graphene and other materials molybdenum disulphide, niobium diselenide and hexagonal boron nitride were first exfoliated from their bulk counterparts.

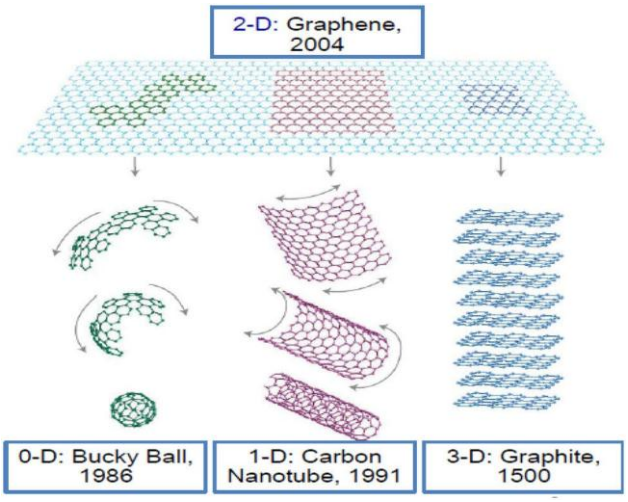

Fig.4.1: Timeline of carbon allotropes

Graphene was first obtained in the form of small flakes of the order of several microns through mechanical exfoliation of graphite using scotch tape [66,67]. Although this method gives the highest quality graphene but for mass production, fabrication method is needed that can synthesize wafer scale graphene.

In recent years, various techniques have been established for graphene synthesis. However, mechanical cleaving (exfoliation) [68], chemical exfoliation [69,70], chemical synthesis [71], and thermal chemical vapor deposition (CVD) [72] synthesis are the most commonly used methods today. Some other techniques are also reported such as unzipping nanotube [73-75] and micro- wave synthesis [76]. Although mechanical exfoliation using AFM cantilever was found capable of fabricating few-layer graphene, the process limitation was thickness of graphene varies to *10 nm, which is comparable to 30-layer graphene.

In chemical exfoliation method, solution dispersed graphite is exfoliated by inserting large alkali ions between the graphite layers. Chemical synthesis is the similar process which consists of the synthesis of graphite oxide, dispersion in a solution, followed by reduction with hydrazine. Similarly for carbon nanotube synthesis, catalytic thermal CVD has proved most significant process for large-scale graphene fabrication. When the thermal CVD process is carried out in a resistive heating furnace, it is known as thermal CVD, and when the process consists of plasma- assisted growth, it is called plasma enhanced CVD or PECVD. In this world as nothing is unmixed blessing, all synthesis methods have some drawbacks too depending upon the final application of graphene. For instance, the mechanical exfoliation method is capable of fabricating monolayer to few-layers of graphene, but the reliability of obtaining a similar structure using this technique is quite insignificant. Furthermore, chemical synthesis processes are low temperature processes that make it more comfort- able to fabricate graphene on multi-types of substrates at ambient temperature, particularly on polymeric substrate. But, large-area synthesized graphene

produced in this process are non-uniform and dispersed. Again, graphene synthesized from reduced graphene oxides (RGOs) usually causes incomplete reduction of graphite oxide that results in the successive debasement of electrical properties depending on its degree of reduction. In contrast, thermal CVD methods are more advantageous for large-area device fabrication and favorable for future complementary metal oxide semiconductor (CMOS) technology by replacing Si [77]. Epitaxial graphene means thermal graphitization of a SiC surface which is another method of graphene synthesis, but the limitations of this method are high process temperature and inability to transfer on any other substrates. So, the thermal CVD method is unique because of producing uniform layer of thermally chemically catalyzed carbon atoms and that can be deposited onto metal surfaces and also can be transferred over a wide range of substrates.

4.1.1 Exfoliation

Basically there are two different approaches to preparing graphene. On the one hand graphene can be detached from an already existing graphite crystal, the so-called exfoliation methods, on the other hand the graphene layer can be grown directly on a substrate surface. The first reported preparation of graphene was by Novoselov and Geim in 2004 [78] by exfoliation using a simple adhesive tape.

4.1.2 The Scotch Tape Method

In this micromechanical exfoliation method, graphene is detached from a graphite crystal using adhesive tape. After peeling it off the graphite, multiple-layer graphene re- mains on the tape. By repeated peeling the multiple-layer graphene is cleaved into various flakes of few-layer graphene. Afterwards the tape is attached to the substrate and the glue solved, e.g. by acetone, in order to detach the tape. Finally one last peeling with an unused tape is performed. The obtained flakes differ considerably in size and thickness, where the sizes range from nanometers to several tens of micrometers for single-layer graphene, depending on the preparation of the used wafer. Single- layer graphene has a absorption rate of 2%, nevertheless it is possible to see it under a light microscope on SiO_2/Si, due to interfer- ence effects [79]. However, it is difficult to obtain larger amounts of graphene by this method, not even taking into account the lack of controllability. The complexity of this method is basically low, nevertheless the graphene flakes need to be found on the sub- strate surface, which is labour intensive. The quality of the prepared graphene is very high with almost no defects.

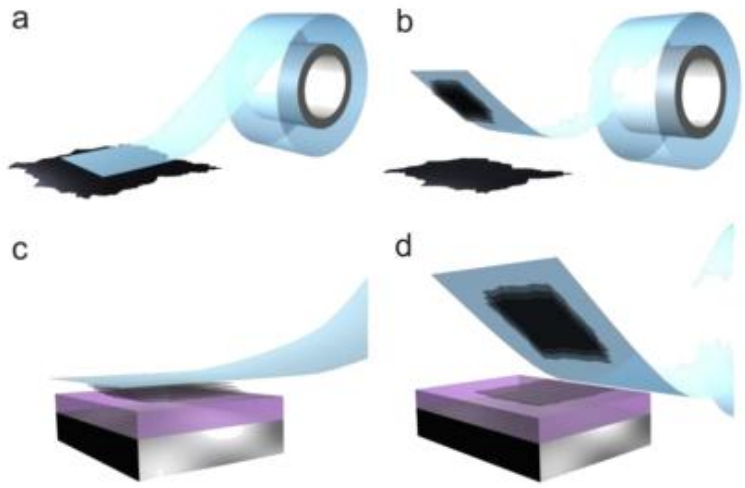

Fig.4.2:Steps in Scotch tape method

4.1.3 Liquid Phase Exfoliation

Liquid-phase exfoliation of graphite oxide is now one of the most widely used methods for preparation of graphene. This method begins with intercalation of graphite with strong oxidizing agents followed by expansion of graphite layers via sonication. The reduction of the obtained graphene oxide to graphene is usually conducted by either thermal or chemical approaches [80-81]. Although this method is capable of high-yield (>50%) production of graphene, the use of large quantity of acid and oxidizing agents requires time-consuming washing steps and produces hazardous wastes. In addition, the vigorous oxidation of graphite often leads to incomplete restoration of the sp2 hybrid carbon bonds and presence of residual oxygen functional groups resulting in poor electrical conductance [82].

4.1.4 Dispersion of Graphite

Graphene can be prepared in liquid-phase. This allows up scaling the production, in order to obtain a much higher amount of graphene. The easiest method would be to disperse the graphite in an organic solvent with nearly the same surface energy as graphite [83]. Thereby, the energy barrier is reduced, which has to be overcome in order to detach a graphene layer from the crystal. The solution is then sonicated in an ultrasound bath for several hundred hours or a

voltage is applied [84]. After the dispersion, the solution has to be centrifuged in order to dispose of the thicker flakes.
The quality of the obtained graphene flakes is very high in accordance with the micromechanical exfoliation. Its size however is still very small, neither is the controllability given. On the other hand, the complexity is very low, and as mentioned above this method allows preparing large amounts of graphene.

4.1.5 Epitaxial Growth

Graphene can be prepared by simply heating and cooling down an SiC crystal [85]. Gen- erally speaking single- or bi-layer graphene forms on the Si face of the crystal, whereas few-layer graphene grows on the C face [86]. The results are highly dependent on the parameters used, like temperature, heating rate, or pressure. In fact, if temperatures and pres- sure are too high the growth of nanotubes in- stead of graphene can occur. The graphitization of SiC was discovered in 1955, but it was regarded as unwelcome side effect instead of a method of preparing graphene [87].The Ni (111) surface has a lattice structure very similar to the one of graphene, with a mismatch of the lattice constant at about 1.3% [87]. Thus by use of the nickel diffusion method a thin Ni layer is evaporated onto a SiC crystal. Upon heating the car- bon diffuses through the Ni layer and forms a graphene or graphite layer on the surface, depending on the heating rate. The thus produced graphene is easier to detach from the surface than the graphene produced by the growth on a simple SiC crystal without Ni [87].

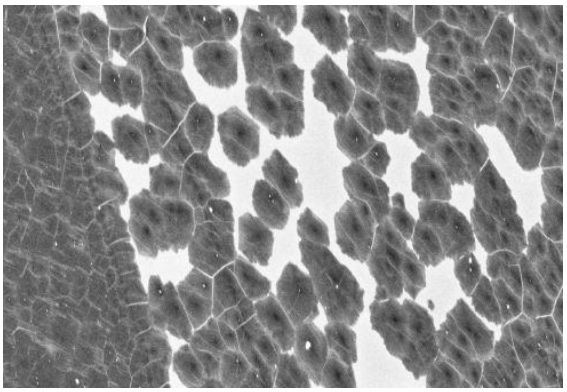

Figure4.3 : SEM image of graphene on copper foil. At several locations on the surface graphene islands form and grow together [89].

The growth of graphene starts at several locations on the crystal simultaneously and these graphene islands grow together, as shown in Fig. 2). Therefore the graphene is not perfectly homogeneous, due to defects or grain boundaries. Its quality therefore is not as good as that of exfoliated graphene, except the graphene would be grown on a perfect single crystal. However, the size of the homogeneous graphene layer is limited by the size of the crystal used. The possibility to pro- duce large amounts of graphene by epitaxial growth is not as good as by liquid-phase exfoliation, though the controllability to gain re- producible results is given. Also the complexity of these methods is comparatively low.

4.1.6 Chemical Vapor Deposition

At present, the process is expensive owing to large energy consumption and because the underlying metal layer has to be removed. However, once the transfer process is optimized this method may indeed be disruptive and cost-effective. A number of issues need to be resolved before graphene CVD technology can become widely used. Graphene growth on thin (tens of nanometres) films of metals needs to be achieved, simultaneously gaining control of the domain (grain) size, ripples, doping level and the number of layers. Control of the number and relative crystallographic orientation of the graphene layers is critical because it will enable a number of applications which would require double, triple and even thicker layers of graphene. Simultaneously, the transfer process should be improved and optimized with the objectives of minimizing the damage to graphene and of recovering the sacrificial metal.

The transfer process might be as complicated as the growth of graphene itself. However, there are a number of applications which rely on conformal growth of graphene on the surface of the metal, and do not require graphene transfer at all: high thermal and electrical conductivities as well as excellent barrier properties allow graphene greatly to enhance the performance of copper interconnects in integrated circuits. Also, because graphene is inert, it is an excellent barrier for any gas, and it forms a conformal layer on metal surfaces with the most complex topographies: such coatings can protect against corrosion.

The game-changing breakthroughs would be the development of graphene growth on arbitrary surfaces and/or at low temperatures (for example, using plasma-enhanced CVD or other methods) with a minimal number of defects. The former would allow one to avoid the complex and expensive transfer step and promote better integration of this 2D crystal with other materials (like Si or GaAs). The latter would improve compatibility with modern microelectronic technologies and allow significant energy saving.

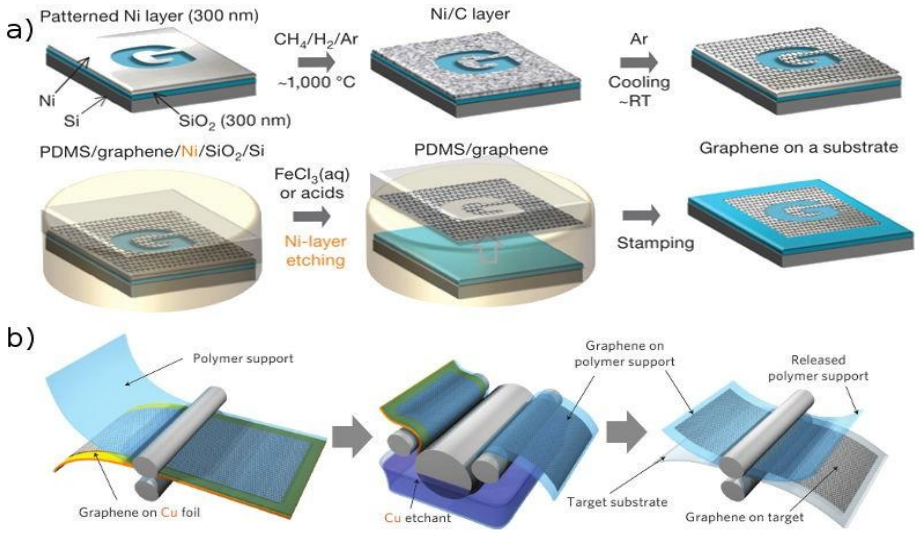

Figure 4.4: **(a)** Scheme of preparation of graphene by CVD and transfer via polymer support. The carbon solves into the Ni during the CVD and forms graphene on the surface after cool- ing. With a polymer support the graphene can be stamped onto another substrate, after etch- ing of the Ni layer. Patterning of the Ni layer allows a control of the shape of the graphene [90].
(b) Roll-to-roll process of graphene films grown on copper foils and transferred on a target substrate [91]

4.1.7 Synthesis on SiC

Silicon carbide is a common material used for high-power electronics. It has been demonstrated that graphitic layers can be grown either on the silicon or carbon faces of a SiC wafer by sublimating Si atoms, thus leaving a graphitized surface[92]Initially, the C-terminated face of SiC was used to grow a turbostratic stack of many randomly oriented polycrystalline layer [96-98]but now the number of graphene layers grown [93,99]can be controlled. The quality of such graphene can be very high, with crystallites approaching hundreds of micrometers in size [94].
The two major drawbacks of this method are the high cost of the SiC wafers and the high temperatures (above 1,000 uC) used, which are not directly compatible with silicon electronics technology. There are potentially several ways to take advantage of the growth of graphene on SiC, including the growth of thin SiC on Si, although this approach requires further development. As a result of the high-temperature growth, high substrate cost, and small-diameter wafers, the use of graphene on SiC.

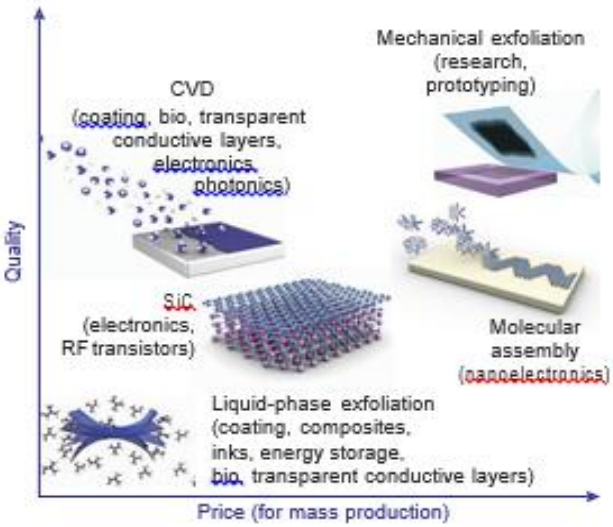

Figure: Several methods of mass-production of graphene, which allow a wide choice in terms of size, quality and price for any particular application[95]

Chapter 5

Graphene Optoelectronics

Optoelectronic devices are electronic devices that use either electric charge to generate light, like light emitting diodes (LED) and lasers, or use light to generate electric current, like photovoltaic devices and photodetectors (PDs). The field can be subdivided into different areas depending on the physical mechanisms responsible for photon or charge generation that are exploited for device operation. Photoemission, radiative recombination, stimulated emission, photoconductivity and the photoelectric effect are examples for the mechanisms that optoelectronic devices might exploit. This review focuses on devices utilizing photoconductivity and the photoelectric effect.
This section reviews optoelectronic devices based on graphene and a major part of the review describes the luminescence and optoelectronics applications based on graphene. Solar cell is a vital optoelectronics application sector to be focused for graphene & GQD. We shall see how graphene & GQD structures are fabricated for the making of solar cells.

5.1 Hybrid solar cells using graphene based transparent electrodes

Pengfei Li and co-workers reported that their work suggests that graphene-based transparent electrode is a promising candidate to replace ITO which is now most popular for making solar cells[100]. The graphene-based transparent and conductive films were demonstrated to be cost-effective electrodes working in organic–inorganic hybrid Schottky solar cells. Large area graphene films were produced by chemical vapor deposition on copper foils and transferred onto glass as transparent electrodes. The hybrid solar cell devices consist of solution- processed poly: poly (PEDOT: PSS), which is sandwiched between silicon wafer and graphene electrode. The solar cells based on graphene electrodes, especially those doped with HNO3, had shown comparable performance to the reference devices using commercial ITO. Graphene has been proposed to be an effective transparent electrode to replace ITO in solar cell [101]as graphene exhibits excel- lent properties such as low-sheet resistance, high transmittance, good mechanical property, and good thermal and chemical solidity[102]. Graphene has very high-carrier mobility as charge carriers in it are delocalized over large areas, resulting in an unencumbered platform for electron/hole transport.

High Fermi-velocity and the ability to be doped chemically contribute to extremely high in-plane conductivities. As early as 2007, Wang et al. (2008)_fabricated polymer solar cells using reduced graphene oxide as transparent electrode and achieved a PCE of 0.26%. After- wards, CVD approach has been used by many groups to synthesize single- or few-layer graphene films with large area for energy harvesting applications, which is a significant advance in this field. Gomez De Arco et al. (2010) reported the continuous, highly flexible, and transparent graphene films produced by CVD as transparent conductive electrodes in organic solar cells. The efficiency of organic solar cells with graphene electrode was 1.18%, which is close to that of organic solar cells with ITO electrode (~1.27%). In 2011, Wang et al. (2011) used layer- by-layer transfer method to fabricate multilayer CVD graphene films with less defects and lower sheet resistance. The organic solar cells with the electrode of four layers graphene have an improved PCE up to 2.5%, which is 83.3% of the PCE of ITO-based devices. For the hybrid solar cell, Wu et al. (2013)_demonstrated the use of graphene as transparent conductive electrodes with the structure of graphene/organic/silicon, which has a PCE of 10%. However, the solar cell has a very small device area of about 0.1 cm*cm. In this work, they had used graphene films as transparent electrodes to work in organic–inorganic hybrid Schottky solar cells with a relatively large device area. The hybrid solar cells based on solution-processed poly : poly PEDOT: PSS in combination with silicon wafer are fabricated through a simple and low cost process (Li et al., 2010; Song et al., 2012; Liu et al., 2013; Shen et al., 2013; Zhu et al., 2013)[103]. It was found that the surface doping of graphene film can effectively improve the device performance. This work had suggested that that the application of graphene based transparent electrode can be extended to a wide range of new optoelectronic devices. Large area graphene films were produced using CVD on the copper foils as the method described in the literature (Yu et al.,2010; Manu et al., 2011). They had used a modified transfer method to formulate the graphene-based transparent electrode.

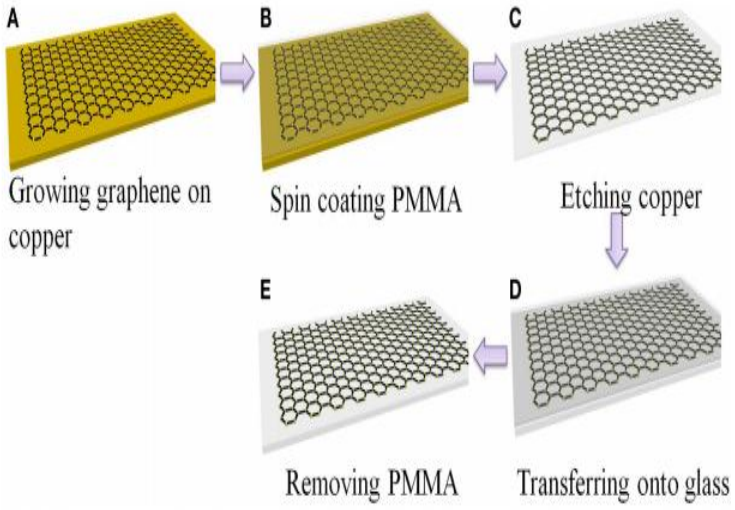

FIGURE 1 | Schematic of transfer graphene onto glass substrate. **(A)** Synthesis of graphene on copper foil, **(B)** spin-coating of PMMA onto the Cu foil to protect graphene, **(C)** etching of Cu, **(D)** transfer of graphene/PMMA film onto glass, **(E)** removal of PMMA in acetone.

The organic–inorganic hybrid solar cells were fabricated by *n* doped Si and PEDOT: PSS. They had used PVD for 0.6 nm of LiF and 200 nm of Al electrode deposition on the back of the silicon wafer. Then PEDOT: PSS had been spin-coated onto the silicon wafer and the graphene/glass. The resulted organic films had then been annealed in a glove box (Shen et al., 2013; Zhu et al., 2013) & the encapsulation of the solar cell devices had included a clamp and AB glue were used to firmly stick the graphene/glass and silicon wafer together. The graphene-based thin films had been successfully applied as transparent electrodes working in organic–inorganic hybrid Schottky solar cells offering comparable photovoltaic performance. It had been found that the chemical doping by HNO3 had effectively increased the work function, reduced the sheet resistance, which in turn improved the solar cell performance. The lifetime study had suggested that graphene based solar cell experienced smaller degradation. For that reason graphene could be a good alternative to ITO in making of solar cells.

5.2 FUNCTIONALIZED LED WITH GQDs

A recent report by Woosung Kwon suggests that chemically derived graphene quantum dots (GQDs) to date had showed very broad emission linewidth due to many kinds of chemical bonding with different energy levels, which significantly degraded the color purity and color tunability. Here, they had showed that use of aniline derivatives to chemically

functionalize GQDs generates new extrinsic energy levels that had led to photoluminescence of very narrow line widths. They had used transient absorption and time-resolved photoluminescence spectroscopies to study the electronic structures and related electronic transitions of our GQDs, which reveals that their underlying carrier dynamics is strongly related to the chemical properties of aniline derivatives. Using those functionalized GQDs as lumophores, they had fabricated light-emitting didoes (LEDs) that exhibit green, orange, and red electroluminescence that has high color purity. The maximum current efficiency of 3.47 cd A−1 and external quantum efficiency of 1.28% are recorded with our LEDs; these are the highest values ever reported for LEDs based on carbon-nanoparticle phosphors. This functionalization of GQDs with aniline derivatives represented a new method to fabricate LEDs with multiple colors.

5.2.1 Synthesis and structural analysis:

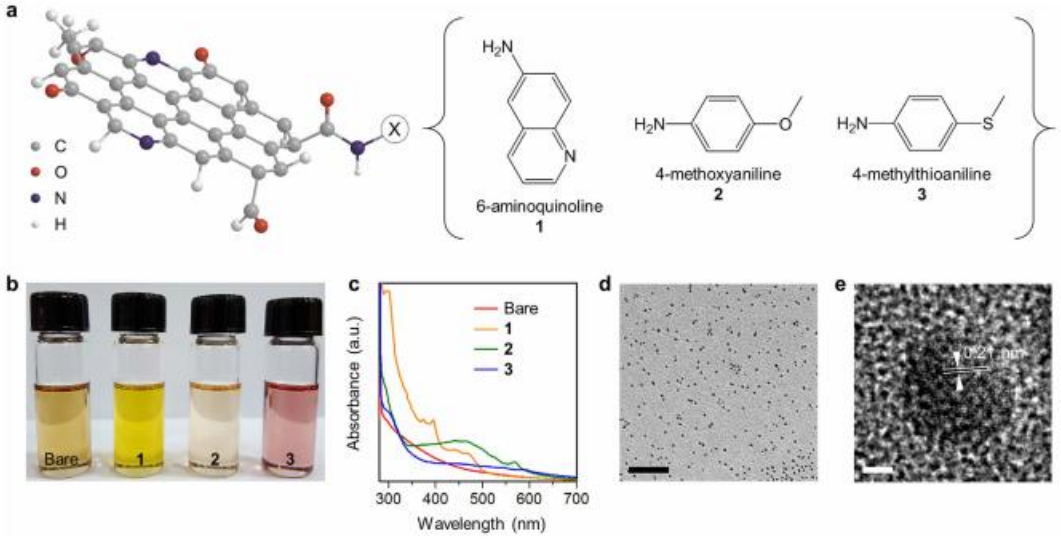

Figure . Synthesis and structural analyses. (**a**) Schematic illustration of the sturcture of GQDs and the chemical structures of aniline derivatives. (**b**) Photograph of solutions of GQDs under daylight. (**c**) Light absorption spectra of GQDs. (**d,e**) Representative TEM images of GQDs show size distribution (scale bar, 100 nm) (**d**) and graphitic structure (scale bar, 2 nm) (**e**).

Graphene quantum dots (GQDs) are graphene derivatives of nanometer size1, 2; they form platelets that have an energy gap that is caused by either quantum confinement or edge effects.These energy gaps give rise to a variety of optical properties, including ultraviolet-to-visible photoluminescence, luminescence upconversion and hot-carrier generation.GQDs can be prepared in many ways but the most common approach is use of chemical

reduction of graphene oxide derived using the Hummers method or its variations .Because almost all reduction processes have limited reducing power, GQDs are likely to preserve "extrinsic" chemical groups, especially oxides and nitrides. Such chemical groups could have many kinds of bonding states with different energy levels, mostly related to nonbonding (*n*) and π orbitals)21(. These energy levels interact with each other to form a variety of energy gaps, some of which generate photoluminescence that has broad linewidth.GQDs have been used as lumophores in light-emitting diodes (LEDs))22(. Son *et al*. demonstrated white LEDs with external quantum efficiency (EQE) = 0.18% by using zinc oxide-graphene quasi-quantum dots23.GQD-LEDs with alkyl amine-terminated GQDs prepared by amidative cutting of graphite generated white light with EQE= ~0.1%24. Use of intercalated graphite has yielded deep-blue GQD-LEDs with luminous efficiency of 0.65 cd A−1. A new approach to transfer water-soluble GQDs into a film realized blue LEDs with low turn-on voltage of 2.5 V (ref. 26). GQDs have also been used as phosphors to convert monochromatic light (usually blue) to white light These results demonstrate the possibility of using GQDs in light-emitting devices, but a main challenge for practical applications is to improve color purity and furthermore to realize green and red light. Color purity is measured as the linewidth of light emission, often specified by full width at half maximum (FWHM). Current GQD-LEDs have very large FWHM> 100 nm, which is responsible for their inferior color purity compared to inorganic quantum dot LEDs. The main reason for such large FWHM is that GQDs have a variety of electronic states and energy gaps due to the presence of residual oxygen or nitrogen (or both) chemical groups. Here, they had reported unprecedented, multicolor light emission from GQDs functionalized with aniline derivatives [105]. The aniline derivatives have no visible photoluminescence in themselves; however, they form very uniform, proper energy gaps through conjugating with GQDs to show green, orange, and red photoluminescence that has narrow linewidth.

They had found that the energy gap was related to the chemical properties of aniline derivatives, and its related electronic transitions were thoroughly studied by means of transient absorption and time-resolved photoluminescence spectroscopies. They had finally demonstrated LEDs that use GQDs functionalized with a series of aniline derivatives to produce green, orange, and red light that has excellent color purity. Bare GQDs were prepared by amidative cutting of graphite oxide as described previously with slight modification24, then chemically functionalized using aniline derivatives: 6-aminoquinoline (**1**), 4-methoxyaniline (**2**), and 4-(methylthio)aniline (**3)** (Fig. 1a; details in Methods). The x-ray photoelectron spectroscopic data (Supplementary Fig. S1) show that the nitrogen content

was increased by 5–10% after functionalization because these aniline derivatives all include an amine group. The sign of carbon-nitrogen (286 eV) bonding was likewise strengthened after functionalization, but the signs of carbon-carbon (284 eV) and carbon-oxygen (288.5 eV) bonding were preserved; this change indicates that the chemical structure of the graphitic core was not changed significantly (Supplementary Fig. S2). We used carbon-13 nuclear magnetic resonance (13C NMR) data to confirm the chemical functionalization with a series of aniline derivatives. Bare GQDs showed chemical shifts of 14.1, 22.7, 31.9, 32.6 (alkyl) and 130.4 ppm (alkene) for the oleyl group and 38.9, 39.1 and 42.8 ppm for amido carbon (Supplementary Fig. S3); these shifts indicate that oleylamine was bonded to carboxylic acid on the edge of GQDs. After functionalization, the spectra of **1**, **2** and **3** all had new lines (Supplementary Fig. S4). **1** showed two new lines, one at 142.5–150.9 ppm and the other at 127.4–137.1 ppm for the pyridine group, which are consistent with 13C NMR lines of 6-aminoquinoline ligand. **2** had four chemical shifts of 55.8 (methoxy), 115.1–115.8, 140.7 and 153.3 ppm (aromatic carbon) which were discovered in the 13C NMR of 4-methoxyaniline ligand. **3** had also four new lines at around 14.8 (methylthio), 127.8, 132.2 and 138.1–145.2 ppm (aromatic carbon), which are associated with 4-(methylthio) aniline ligand. However, **1**, **2** and **3** all retained the oleyl and amido shifts; this observation indicates that the aniline derivatives bonded to vacancies rather than replace oleylamine. This replacement would be difficult because it requires breaking amide bonds, which is difficult in our experimental conditions. Infrared spectroscopy (Supplementary Fig. S5) showed that **1**,**2** and **3** had C= O stretching (1500–1400 cm−1) and C–N stretching (1350–1250 cm-1) bands, and preserved a trace of the C–H stretching (3000–2900 cm−1) and N–H stretching (3500-3000 cm−1) bands, which all could be attributed to oleylamine on the edge of GQDs.After functionalization, the sample colors (Fig. 1b) were significantly changed due to the development of new light absorption bands in the range of 400–600 nm (Fig. 1c). Transmission electron microscopy (TEM) images show that the size of our GQDs is ~3 nm, and because of the presence of ligand molecules, the GQDs did not agglomerate.

5.2.2 Photoluminescence excitation and emission spectroscopy

To investigate the effect of functionalization on the energy gap of our GQDs, they had conducted photoluminescence excitation and emission spectroscopy measurements (Fig. 2). The excitation spectrum of bare GQDs consists of a single peak at wavelength λ= 350 nm, which corresponds to photon energy of 3.54 eV (Fig. 2a). This electronic transition may be associated with *n* orbitals of oxygen and nitrogen atoms in GQDs21,22,24,28, i.e., their *n* electrons were pumped into π* orbitals of graphitic units of GQDs by excitation light. The broad linewidth may be a result of the variety of oxygen and nitrogen chemical structures on the GQDs. Because the energy level of *n* orbitals is substantially influenced by bonding states and surroundings, the bare GQDs had many different energy gaps, each of which interacted with a specific range of excitation light; as a result, the emission linewidth was broad because it is the sum of many lines. Functionalization of GQDs with aniline derivatives resulted in excitation bands in the visible region up to $\lambda \sim$ 600 nm (Fig. d). These bands were composed of multiple, discrete peaks; this pattern resembles the vibrational structure of electronic transitions in dye molecules.

This result suggests that the electronic structures of functionalized GQDs are largely influenced by molecule-like, discrete energy levels of the aniline derivatives. It had three major peaks (λ= 300, 380 and 460 nm) (Fig. b); their broad linewidths can be attributed to the large number of vibrational modes in the quinoline unit 29. In connection with their light absorption spectra (Fig. 1c), the peak at λ= 300 nm can be assigned to the π → π* transition, and the peak at λ= 460 nm can be assigned to the *n*→ π* transition. **2** had a sharp peak at $\lambda \sim$300 nm that represents the π → π* transition, and a structured band at 450≤ λ≤ 570 nm that consists of peaks spaced at intervals of ~40nm (Fig. 2c), and represents the *n*→ π* transition. These two transitions are separated by a forbidden gap; i.e., the functionalized GQDs have the discrete energy levels. **3** also exhibits a π → π* peak at λ= 305 nm and *n*→ π* band at 470≤ λ≤ 590 nm (Fig. 2d). Its *n*→ π* band position is red-shifted by 20 nm with respect to **2**, presumably because sulfur atoms near positive carbon in **3** can act as a stronger π donor than oxygen atoms in **2** and may possibly result in a bathochromic shift30. The emission spectrum of bare GQDs shows a long-tailed, asymmetric peak at λ= 420 nm (Fig. 2e). This typical peak shape has been considered to indicate that GQDs possess various photoluminescence centers that have distinct chemical structures and correspondingly different singlet ground (S0)–first-excited state (S1)gaps31,32.After functionalization, **1** exhibits a relatively narrow, single peak (FWHM ~50 nm) at λ= 510 nm (Fig. 2f). The peak position remained constant regardless of excitation light; i.e., Kasha's rule was met. The emission spectrum of **2** shows a very narrow

peak (FWHM ~20 nm) at λ= 570 nm with a minor peak at λ= 620 nm (Fig. g). This double-peaked photoluminescence has been often observed in polyaromatic systems and in our case, the energy difference (~0.1 eV) may correspond to the C–C inter-ring or intra-ring stretch modes. Similarly, **3** had a major peak at λ= 605 nm and a minor peak at λ= 655 nm (Fig. 2h). The similarity between the emission spectra of **2** and **3** may be due to the similarity in their ligands. The photograph of the photoluminescence of our GQDs is shown in Figure.

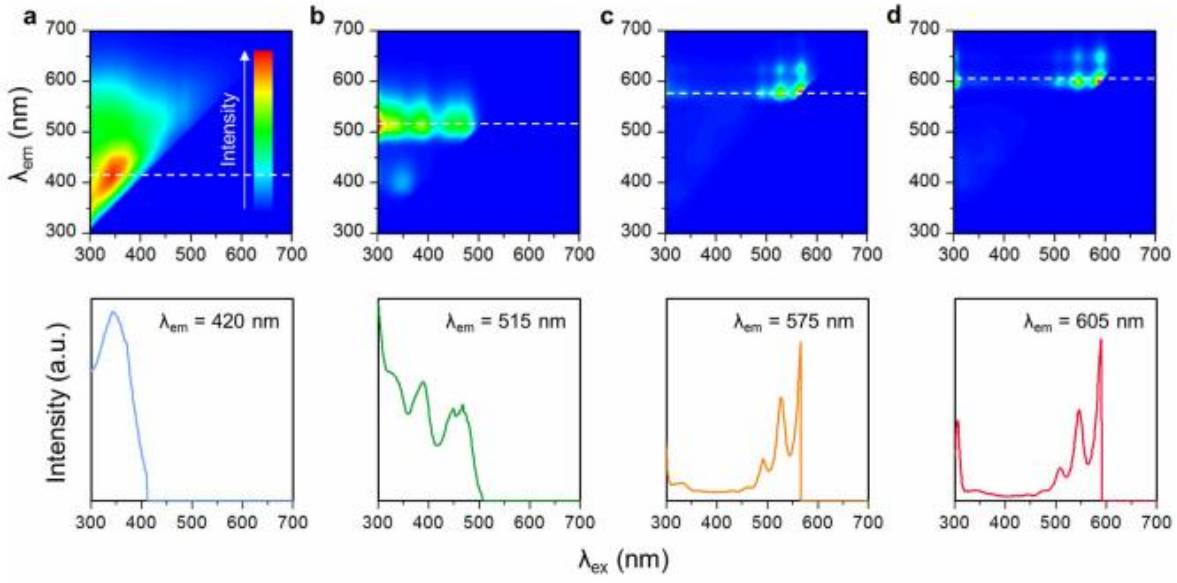

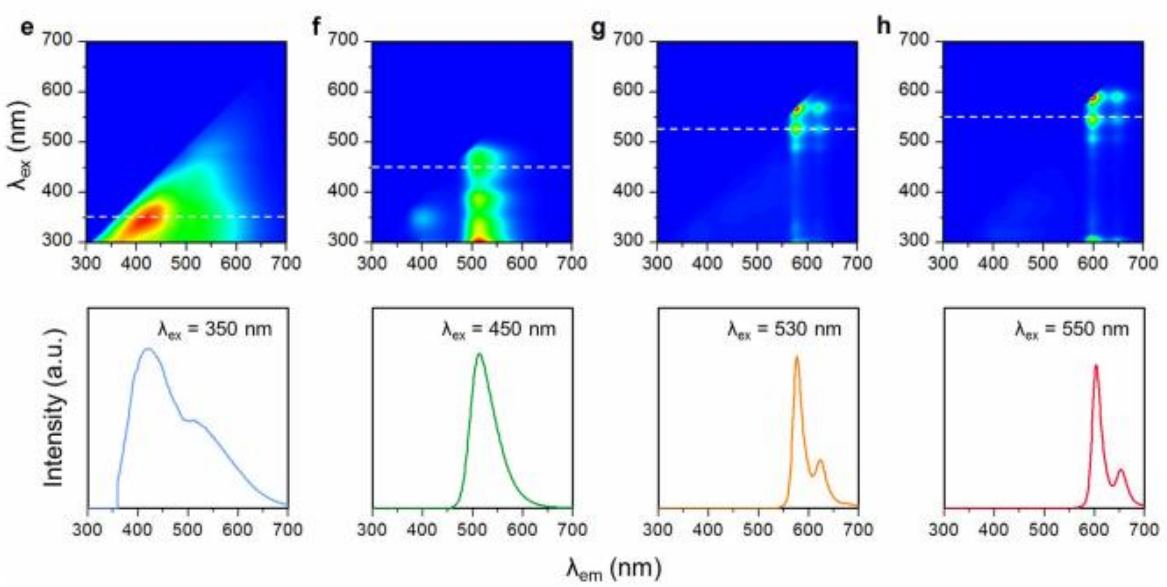

Figure . Photoluminescence spectroscopy. (**a–d**) Photoluminescence excitation contour maps and corresponding cross-sectional spectra at specific emission wavelengths λ_{em} of bare GQDs (**a**), **1** (**b**), **2** (**c**), and **3** (**d**). (**e–h**) Photoluminescence emission contour maps and corresponding cross-sectional spectra at specific excitation wavelengths λ_{ex} of bare GQDs (**e**), **1** (**f**), **2** (**g**), and **3** (**h**). Dotted lines indicate wavelengths at which cross-sectional spectra are obtained.

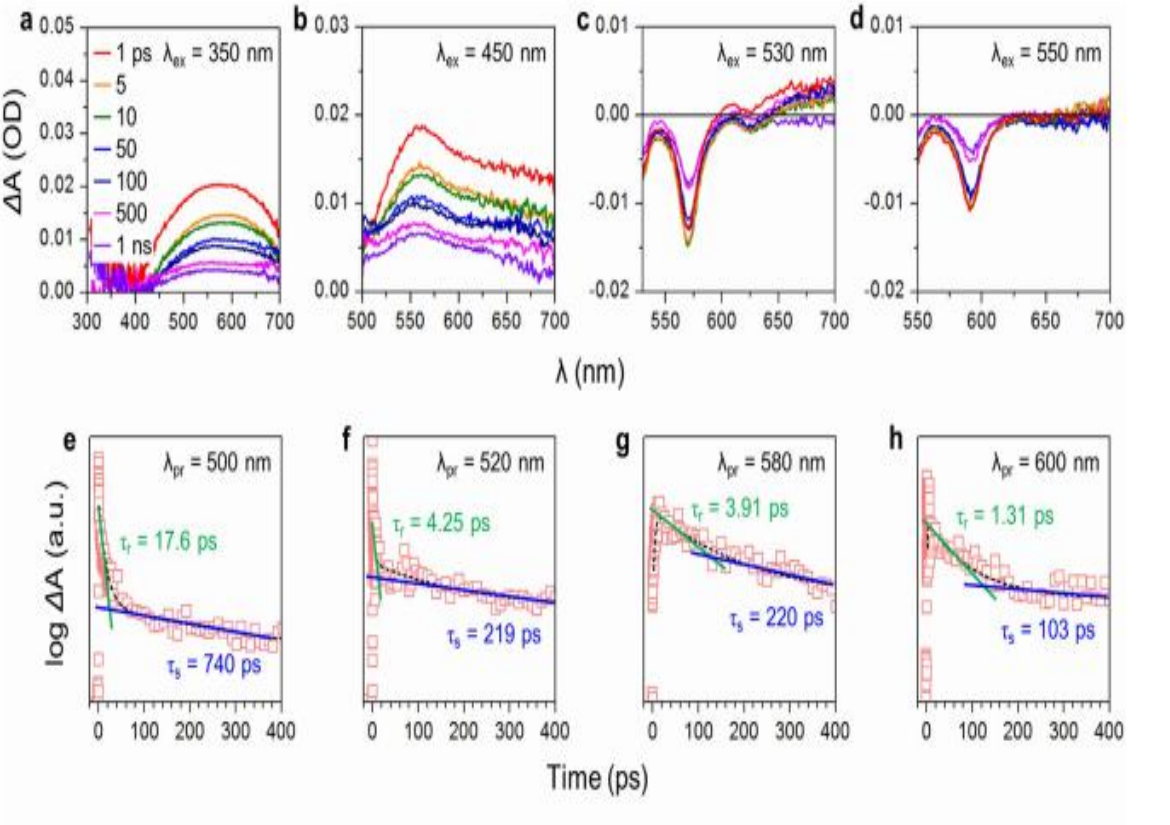

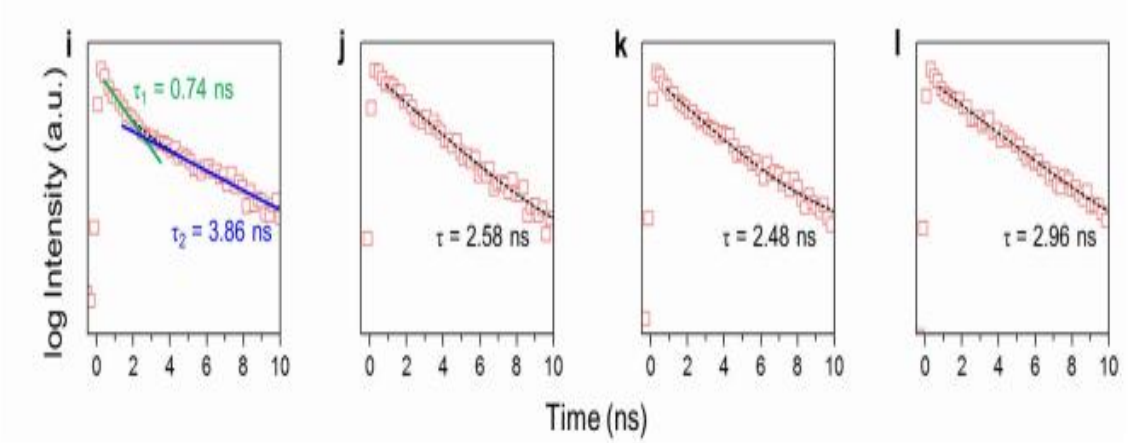

Figure . Transient absorption and time-resolved photoluminescence spectroscopy. (**a–d**) Transient absorption spectra at specific excitation wavelengths λ_{ex} and (**e–h**) corresponding time-correlated excited-state electron decay profiles at specific probe wavelengths λ_{pr} of bare GQDs (**a**,**e**), **1** (**b**,**f**), **2** (**c**,**g**), and **3** (**d**,**h**). (**i–l**) Time-resolved photoluminescence spectra at specific excitation wavelengths (λ_{ex}) of bare GQDs (**e**), **1** (**f**), **2** (**g**), and **3** (**h**).

5.2.3 LED Demonstration

They had demonstrated LEDs that use 1, 3,5tris (Nphenylbenzimidizol-2-yl) benzene (TPBI): tris (4-carbazoyl-9-ylphenyl) amine (TCTA) in 1:1 weight ratio as a co-host, and our functionalized GQDs as a dopant in an emitting layer (EML) (Fig. 4a). The concentrations of **1**, **2**, and **3** in the host matrix were 10,20, and 20 wt%, respectively. Each device also included a self-organized polymeric hole injection layer (SOHIL), which is composed of a conventional poly (3, 4-ethylenedioxythiphene): poly (styrene sulfonate) (PEDOT: PSS)and per fluorinated polymeric acid, tetra-fluoroethylene-perfluoro-3,6-dioxa-4-methyl-7-octene-sulfonic acid copolymer (PFI)38–41. Due to self-organization of PFI during spin coating, the SOHIL has a work function that increases gradually from 5.2 eV at the bottom to 5.95 eV at the top[104]; this gradient induces efficient hole injection into EML (TCTA:TPBI:GQD) by reducing the hole-injection barrier. The large proportion of PFI at the top of the SOHIL also prevents exciton quenching at the interface between PEDOT: PSS and EML, and consequently increases the luminescence efficiency of devices40, 41. Under a certain electrical bias, electrons are pumped through Al/LiF/TPBI cathodes and holes are injected through ITO/SOHIL anodes (Fig. 4b). These injected carriers are then

transferred into a co-host system in the EML. The co-host system that incorporates hole-transporting TCTA and electron-transporting TPBI has facilitated direct carrier injection by broadening the recombination zone42, which can increase the device efficiency, and generate a pure electroluminescence spectrum from GQD dopants. For functionalized GQDs, the highest occupied molecular orbital (HOMO) levels were determined by means of ultraviolet photoelectron spectroscopy (Supplementary Fig. S14) and the lowest unoccupied molecular orbital (LUMO) levels were deduced from Kelvin probe analysis results (Supplementary Fig. S15) and photoluminescence excitation onset wavelengths (details in Supplementary Information). The emission spectra of the LEDs were affected by the functionalization. The host-only LEDs emitted deep blue light (peak at λ= 460 nm, FWHM= 60 nm; Fig. 4c); Lmax= ~100 cd m−2 and EQE= ~0.4% were achieved at 10 V (Fig. 4g; Supplementary Fig. S16). The Commission Internationale de l'Éclairage (CIE) coordinates were (0.192, 0.212; Supplementary Fig. S17). The LEDs employing 1 emitted green light (peak at λ= 510 nm,FWHM= 80 nm; Fig. 4d) with Lmax= 390 cd m−2 and EQE= 1.28% (Fig. 4h; Supplementary Fig. S18). The CIE coordinates were (0.286, 0.496; Supplementary Fig. S19). The electroluminescence spectra of 1-LEDs overlapped the photoluminescence spectrum and was not affected by applying bias (Supplementary Fig. S18); these traits indicate that the TCTA:TPBI co-host efficiently transfers carriers into 1. To our best knowledge, this is the highest efficiency ever reported for LEDs based on carbon nanoparticles as a phosphor (Supplementary Information, Table S5). The electroluminescence spectrum of the 2-LEDs shows two peaks: a major one at λ= 590 nm and a lesser one at λ= 630 nm, where FWHM of the major peak is ~50 nm (Fig. 4e). This device showed Lmax= ~3 cdm−2 and EQE = ~0.1% (Fig. 4i; Supplementary Fig. S20). The CIE coordinates were (0.567, 0.432), which is located at around the color boundary between orange and amber (Supplementary Fig. S21). The 3-LEDs emitted red light (peak at λ= 620 nm, FWHM ~50 nm; Fig. 4f) with Lmax= ~2 cd m−2 and EQE= ~0.1% . The CIE coordinates were (0.682, 0.318), which indicate that the emission color was very saturated and pure.

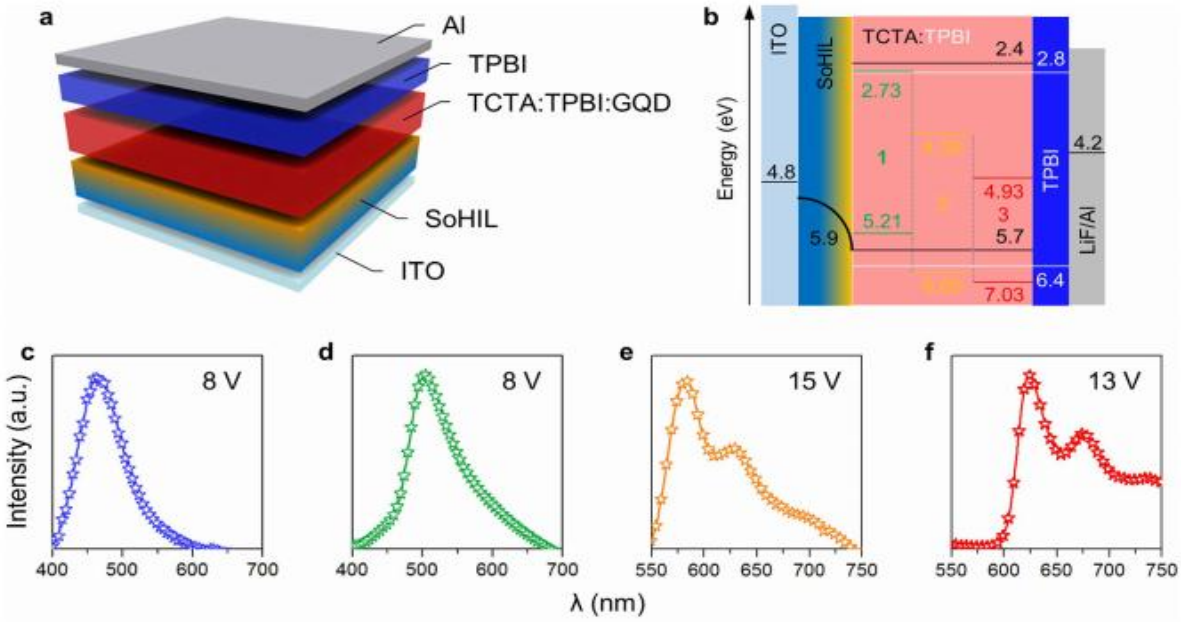

Figure 4. LED demonstration. (**a**) Structure of LEDs. (**b**) Energy levels in LEDs. (**c–f**) Electroluminescence spectra (top) and photographs (bottom) of host-only (**c**), **1**- (**d**), **2**- (**e**), and **3**-LEDs (**f**). Current density and luminance of host-only

Recent trials to demonstrate GQD-based LEDs have achieved a considerable success, but a remaining major challenge is to achieve high color purity (i.e., narrow linewidth of emitted light). To overcome these challenges, they had chemically functionalized GQDs with a series of aniline derivatives. After this functionalization, our GQDs showed dramatic narrowing of photoluminescence linewidths. This improvement could be attributed to the formation of new extrinsic energy levels as a result of interaction between intrinsic energy levels of GQDs and aniline derivatives. Due to these extrinsic energy levels, the LEDs that use our functionalized GQDs as lumophores exhibited green, orange, and red electroluminescence that has narrow linewidths (FWHM< 80 nm) and high color purity. The best Lmax= 390 cd m^{-2} and EQE= 1.28% (current efficiency= 3.47 cd A^{-1}) were recorded with their green LED. Our devices are still inferior to the state-of-the-art LEDs based on inorganic quantum dots; however, considering resource depletion and environmental pollution related to use of rare-earth and heavy metals, these functionalized GQDs may have strong potential as clean light sources in future displays.

5.3 Si Hybrid solar cells using GQDs:

In a report by Meng-Lin Tsai by employing GQDs in PEDOT: PSS, they had achieved an efficiency of 13.22% in Si/PEDOT: PSS hybrid solar cells. The efficiency enhancement was based on concurrent improvement in optical & electrical properties by the photon down conversion process and the improved conductivity of PEDOT: PSS via appropriate incorporation of GQDs. After introducing GQDs into PEDOT:PSS, the short circuit current and the fill factor of rear-contact optimized hybrid cells are increased from 32.11 to 36.26 mA/cm*cm & 62.85% to 63.87%, respectively. The organic−inorganic hybrid solar cell obtained herein held the promise for developing photon-managing, low-cost, & highly efficient photovoltaic devices.

5.3.1 Fabrication Process

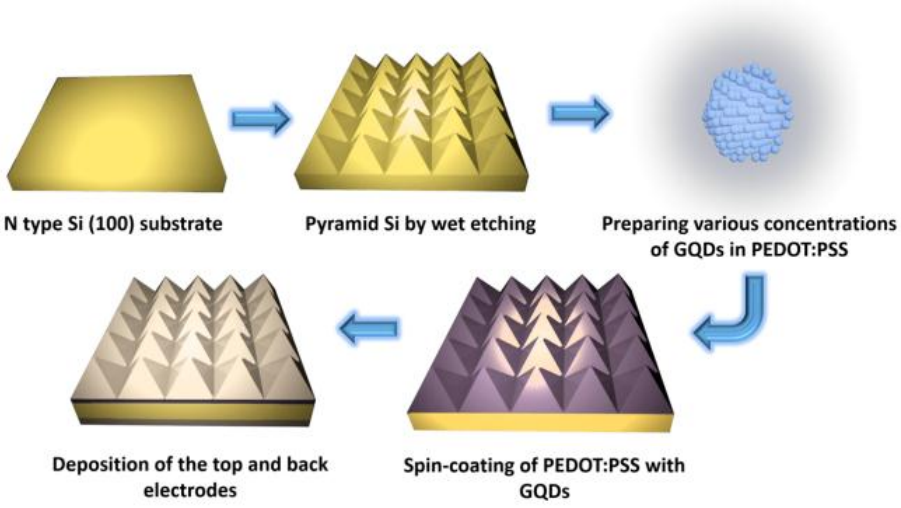

Figure . Fabrication process of PEDOT:PSS/Si hybrid solar cells with GQDs.

In this process, the introduction of GQDs to PEDOT:PSS for PEDOT:PSS/Si organic−inorganic hybrid solar cells leads to the increase of JSC from 32.11 mA/cm2 to 36.26 mA/cm*cm & FF from 62.85% to 63.87% due to combined effects of photon down conversion and improved conductivity of the PEDOT:PSS layer by GQDs. The concurrent improvement in optical & electrical properties due to the introduction of GQDs gives rise to a world-record high PCE of 13.22% among all the reported Si/organic hybrid solar

cells. The realization of high-efficiency hybrid solar cells demonstrated here makes GQDs attractive for large-area and cost-effective cells.

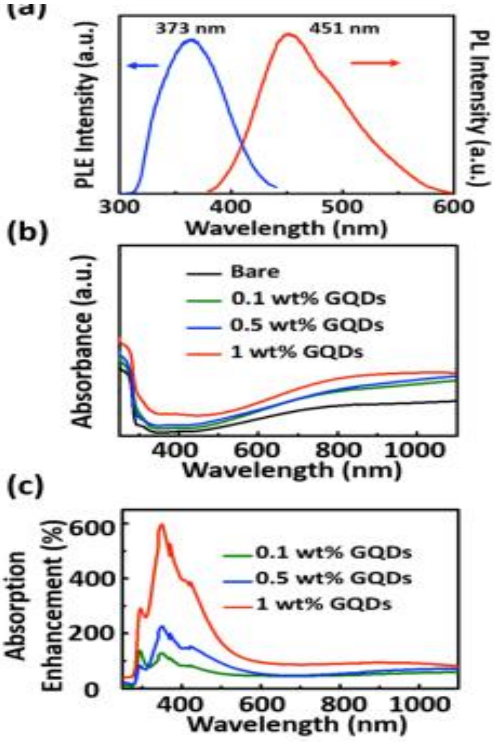

Figure . (a) PLE (left) and PL (right) spectra of GQDs. (b) Absorbance spectra of PEDOT:PSS layers without GQDs and with 0.1, 0.5, and 1 wt % of GQDs on glass substrates. (c) Absorption enhancement of PEDOT:PSS layers with 0.1, 0.5, and 1 wt % of GQDs on glass substrates.

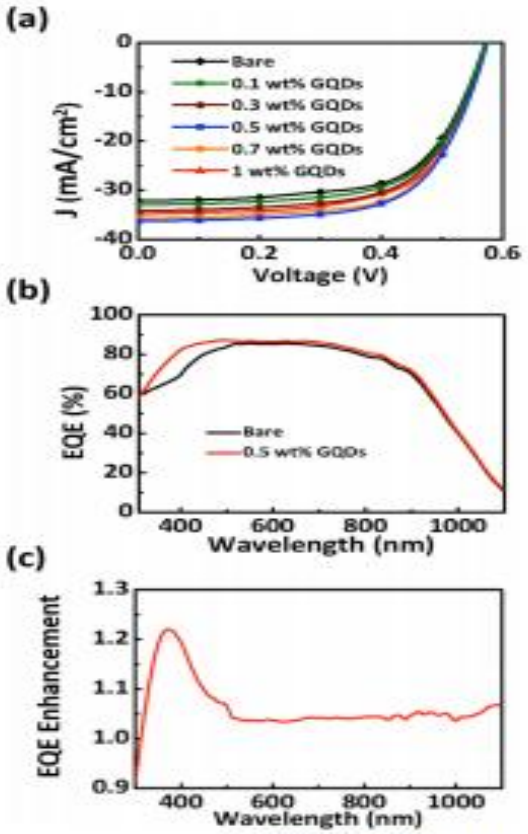

Figure . (a) *J–V* characteristics of PEDOT:PSS/Si hybrid solar cells without GQDs and with 0.1, 0.3, 0.5, 0.7, and 1 wt % of GQDs. (b) EQE spectra of PEDOT:PSS/Si hybrid solar cells without GQDs and with 0.5 wt % of GQDs. (c) EQE enhancement of PEDOT:PSS/Si hybrid solar cells with 0.5 wt % as compared to cells without GQDs.

They had successfully fabricated Si/PEDOT:PSS hybrid solar cells with an efficiency up to 13.22% by concurrent improvement in optical and electrical properties via the down conversion effect and enhanced conductivity of PEDOT: PSS due to introduction of GQDs. The low-cost, photon-managing and high-performance device design based on low-temperature solution processes holds the promise for more cost-effective Si based optical devices.

Chapter 6

Future Aspects

Graphene is called the wonder material just because of its tremendous properties in Nanoelectronics, Optoelectronics, Photonics, Mechanical applications etc. Basically, Graphene provided the excitement and invigorated the researchers to explore isolated 2D atomic layers other than graphene that have a rich variety of composition, electronic structures and properties. The journey of 2D materials is divided into 2 sections that is Graphene and beyond graphene. The need for the exploration beyond graphene was some shortcomings of graphene and the most prominent one was and still is the band gap problem of graphene which hindered it to work as a replacement of semiconductors. There is no significant band gap between the conduction and valence band of graphene and band gap engineering is somewhat impossible as it is a single layered structure. The problems with graphene are mainly the cause for the emergence of other 2D materials.

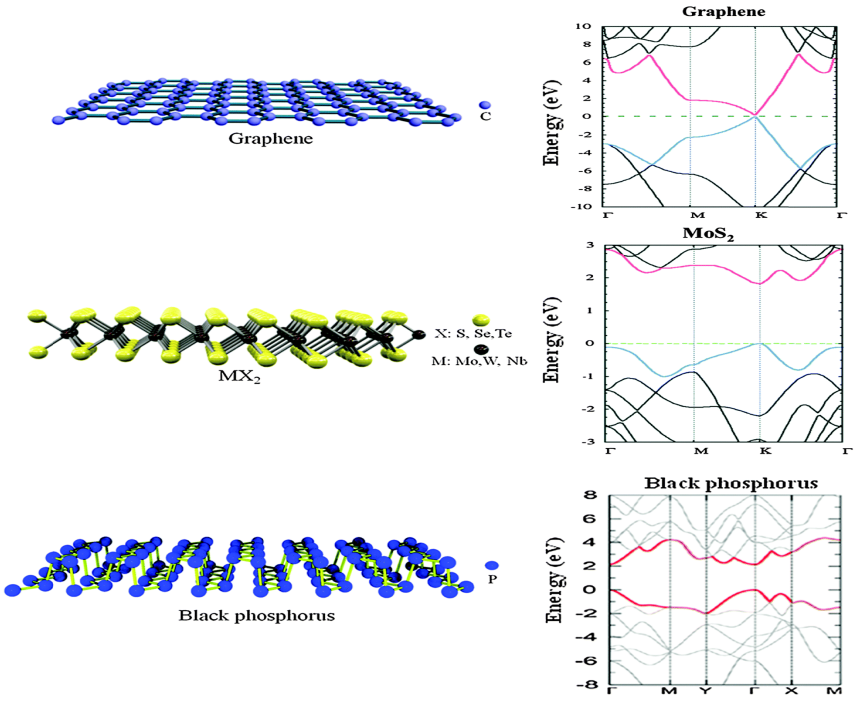

Figure6.1:Bandgap in 2D material family

Beyond the study of graphene in the past decade, the discovery of other two-dimensional (2D) materials, like hexagonal-Boron Nitride (h-BN) and Molybdenum Disulfide (MoS_2), $MoSe_2$, $NbSe_2$ Transition Metal Dichalcogenides(TMDCs) etc. have opened new doors in materials science and condensed matter physics. There is opportunity to engineer the band gaps in these 2D atomic layers to span the entire range of materials from metals to semiconductors to insulators. Further, combing 2D materials with distinct properties into heterostructures that is combining leyer on top of each other of different 2D materials or engineering their shape and size on the nanoscale provides a scientific and technological dreamscape to explore new physics and create new functionality. More importantly, such new classes of 2D materials offer large playgrounds of rich unprecedented physics.In case of luminescence applications, Researchers are not relying on graphene only nowadays.Rather,they are tilting towards other members of 2D material family as some of them offer tunable bandgap and some offer large enough bandgap that meet the requirement of certain optoelectronic applications. But scientists working with graphene are adamant to work with graphene in future as well and introduce tunable bandgap in graphene to meet the demand of luminescence applications.

Chapter 7

Conclusion

Graphene is a unique crystal in the sense that it combines many superior properties, from mechanical to electronic. This suggests that its full power will only be realized in novel applications, which are designed specifically with this material in mind, rather than when it is used to replace other materials in existing applications. Interestingly, such an opportunity is likely to be provided very soon with development of such new technologies as printable and flexible electronics, LEDs, flexible solar cells, touch screens etc. The main hindrance towards luminescence application that is zero band gap in graphene has been addressed and some advances in introducing bandgap in graphene has been reviewed in this work.

The reconfigurability of its optical properties together with its ease of fabrication and integration has enabled the possibility to construct optoelectronic devices and systems based on graphene. Recent progress on optoelectronic devices based on this emerging material and one of its derivative graphene quantum dots were reviewed and discussed.Physicists are used to thinking of graphene as a perfect two-dimensional lattice of carbon atoms. However, the paradigm is now shifting as pure science opens new technology routes: even less-than-perfect layers of graphene can be used in certain applications. In fact, different applications require different grades of graphene, bringing closer widespread practical implementation of this material. Although still in an early stage of development, the performance of these devices is already approaching that of state-of-the-art current technologies.

References

[1] S. Park and R. S. Ruoff,Nat. Nanotechnol., 2009, 4, 217–224.

[2] A. K. Geim and K.S. Novoselov, "The rise of graphene," Nature Materials, vol. 6, no. 183,2007.

[3] A.K. Geim, "Graphene: Status and Prospects," Science, vol.324,no.5934, p.1530,June,2009.

[4] Yuanbo Zhang et al, "Experimentla Observation of the quantum Hall effect and Berry's phase in graphene," Nature, vol. 438,pp.201-204,September 2005.

[5] M Scarselli et al, "Electronic and Optoelectronic nano-devices based on carbon nanotubes," Journal of Physics: Condensed Matter, vol.24, no. 31, 2012.

[6] L.G. Wade, Organic Chemistry (5th Edition): Prentice Hall,.2002

[7] A.H.Castro Netoetal, "The electronic properties of graphene," Rev.Mod.Phys,vol. 81, no. 109, Jan. .2009

[8] Peres N M R 2010 Colloquium: the transport properties of graphene: an introduction Rev. Mod. Phys. 82 2673–700.

[9] Peres N M R, Guinea F and Castro Neto A H 2006 Electronic properties of disordered two-dimensional carbon Phys. Rev. B 73 125411

[10] Mak K F, Sfeir M Y, Wu Y, Lui C H, Misewich J A and Heinz T F 2008 Measurement of the optical conductivity of graphene Phys. Rev. Lett. 101 196405

[11] Geim A K, Nair R R, Blake P, Grigorenko A N, Novoselov K S, Booth T J, Stauber T and Peres N M R 2008 Fine structure constant defines visual transparency of graphene Science 320 1308

[12] Winnerl S et al 2011 Carrier relaxation in epitaxial graphene photoexcited near the Dirac point Phys. Rev. Lett. 107 237401

[13] Z. Q. Li, E. A. Henriksen, Z. Jiang, Z. Hao, M. C. Martin, P. Kim,H. L. Stormer, and D. N. Basov, "Dirac charge dynamics in graphene by infrared spectroscopy," *Nature Phys.*, vol. 4, no. 7, pp. 532–535, 2008.

[14] F. Wang, Y. Zhang, C. Tian, C. Girit, A. Zettl, M. Crommie, and Y. Ron Shen, "Gate-variable optical transitions in graphene," *Science*, vol. 320, no. 5873, pp. 206–209, 2008.

[15] B. Sensale-Rodriguez, R. Yan, L. Liu, D. Jena, and H. G. Xing, "Graphene for reconfigurable terahertz optoelectronics,"Proc. IEEE, vol. 101, no. 7, pp. 1705–1716, Jul. 2013.

[16] K. Yang, S. Arezoomandan, and B. Sensale-Rodriguez, "The linear and nonlinear THz properties of graphene," *Terahertz Sci. Technol.*, vol. 6, no. 4, pp. 223–233, 2013.

[17] F. Bonaccorso, Z. Sun, T. Hasan, and A. C. Ferrari, "Graphene pho- tonics and optoelectronics," *Nature Photon.*, vol. 4, no. 9, pp. 611–622, 2010.

[18] Q. Bao and K. P. Loh, “Graphene photonics, plasmonics, and broadband optoelectronic devices,” *ACS Nano*, vol. 6, no. 5, pp. 3677–3694, 2012.
[19] A.K. Geim, K.S. Novoselov, The rise of graphene, Nat. Mater .191-183 (2007) 6
[20] K. Kim, J.Y. Choi, T. Kim, S.H. Cho, H.J. Chung, A role for graphene in siliconbased semiconductor devices, Nature .344-338 (2011) 479
[21] Gierz I, Riedl C, Starke U, Ast C R and Kern K 2008 Atomic hole doping of grapheneNano Lett.84603–7
[22] Coletti C, Riedl C, Lee D S, Krauss B, Patthey L,von Klitzing K, Smet J H and Starke U 2010 Charge neutrality and band-gap tuning of epitaxial graphene on SiC by molecular doping Phys. Rev.B81235401
[23] Li X, Wang X, Zhang L, Lee S and Dai H 2008 Chemically derived, ultrasmooth graphene nanoribbon semiconductors Science3191229–32
[24] Elias E C et al. Control of graphene’s properties by reversible hydrogenation: evidence for graphene Science323610,–3,2009
[25] Jaiswal M, Lim C H Y X, Bao Q, Toh C T, Loh K P and Özyilmaz B, Controlled hydrogenation of grapheme sheets and nanoribbonsACS Nano5888–96,2011
[26] Wang F, Liu G, Rothwell S, Nevius M, Tejeda A,Taleb Ibrahimi A, Feldman L C, Cohen P I and Conrad E H Wide-gap semiconducting graphene from nitrogenseeded SiC Nano Lett.134827–32,2013
[27] Takahashi T, Sugawara S, Noguchi E, Sato T and Takahashi T Band-gap tuning of monolayer graphene by oxygena dsorption Carbon73141–5,2014
[28] Balog R et al Bandgap opening in graphene induced by patterned hydrogen adsorptionNat. Mater.9315–9,2010
[29] Berashevich J and Chakraborty T Tunable band gap and magnetic ordering by adsorption of molecules on grapheme Phys. Rev.B80033404,,2009
[30] E. J. Duplock, M. Scheffler and P. J. D. Lindan,Phys. Rev.Lett., 92, 225502,2004
[31] Y. W. Son, M. L. Cohen and S. G. Louie,Phys. Rev. Lett., 97, 216803,2006
[32] X. Liang, Z. Fu and S. Y. Chou,Nano Lett., 7, 3840,2007,
[33] Y.-M. Lin, C. Dimitrakopoulos, K. A. Jenkins, D. B. Farmer, H.-Y. Chiu, A. Grill and P. Avouris,Science, 327, 2010 ,662
[34] F. Xia, D. B. Farmer, Y.-M. Lin and P. Avouris,Nano Lett., 10, 715,2010
[35] sung et al.(2 ta jabe)
[36] A. J. Gr¨ uneis,J. Phys.: Condens. Matter, 25, 043001,2013
[37] Y. Zhang, T. Tang, C. Girit, Z. Hao, M. Martin, A. Zettle, M. F. Crommie, Y. Shen and F. Wang,Nature, 459, 820,2009
[38] S. J. Sung, P. R. Lee, J. G. Kim, M. T. Ryu, H. M. Park and J. W. Chung, Appl. Phys. Lett., 105, 081605,2014
[39] N. Li, G. Lee, J. W. Yang, H. Kim, M. S. Yeom,
[40] R. H. Scheicher, J.-S. Kim and K.-S. Kim,J. Phys. Chem. C,117 , 4309,2013
[41] S. J. Sung, P. R. Lee, J. G. Kim, M. T. Ryu, H. M. Park, and J. W. Chung, Band gap engineering for graphene by using Na+ions, APPLIED PHYSICS LETTERS105, 081605,(2014)
[42] Sung etal.Band modification of graphene by using slow Cs+ ions, RSC Adv.,2016,6,9106,(2015)

[43] D. Usachov, O. Vilkov, A. Grüneis, D. Haberer, A. Fedorov, V.K. Adamchuk, et al., Nitrogen-doped graphene: efficient growth, structure and electronic properties, Nano Lett. 2011 ,5407-5401 11
[44] K. Watanabe, T. Taniguchi, H. Kanda, Direct-bandgap properties and evidence for ultraviolet lasing of hexagonal boron nitride single crystal, Nat. Mater -404 3 (2004),409
[45] M. Kan, J. Zhou, Q. Wang, Q. Sun, P. Jena, Tuning the band gap and magnetic properties of BN sheets impregnated with grapheneflakes, Phys. Rev. B ,(2011)84 .205412
[46] P.P. Shinde, V. Kumar, Direct band gap opening in graphene by BN doping:Ab initio calculations, Phys. Rev. B .125401 (2011) 84
[47] X. Fan, Z. Shen, A.Q. Liu, J.L. Kuo, Bandgap opening of graphene by doping small boron nitride domains, Nanoscale 2165-2157 (2012)
[48] L. Ci, L. Song, C. Jin, D. Jariwala, D. Wu, Y. Li, et al., Atomic layers of hybridized boron nitride and graphene domains, Nat. Mater .435-430 (2010)
[49] C.K. Chang, S. Kataria, C.C. Kuo, A. Ganguly, B.Y. Wang, J.Y. Hwang, et al., Bandgap engineering of chemical vapor deposited graphene byin-situ BN doping, ACS Nano .1341-1333 (2013)
[50] G.C. Loh, R. Pandey, A grapheme boron nitride lateral heterostructure, J. Mater. Chem. C .5918 ,(2015)
[51] P. Nath, S. Chowdhury, D. Sanyal, D. Jana, Ab-initio calculation of electronic and optical properties of nitrogen and boron doped graphene nanosheet, Carbon 73 .282-275 ,(2014)
[52] R. Nascimento, J. da R. Martins, R.J.C. Batista, H. Chacham, Band gaps of BNdoped graphene fluctuations, trends, and bounds, J. Phys. Chem. C ,(2015)119 .5061-5055
[53] L. Ferrighi, M.I. Trioni, C.D. Valentin, Boron-doped, nitrogen-doped and codoped graphene on Cu(:(111a DFT-VdW study, J. Phys. Chem. C 119 6064-6056,(2015)
[54] P. Rani, V.K. Jindal, Designing band gap of graphene by B and N dopant, RSC Adv. 3 (2013) 802.
[55] Z.M. Liu, Y. Zhu, Z.Q. Yang, Half metallicity and electronic structures in armchair BCN-hybrid nanoribbons, J. Chem. Phys. 134 (2011) 074708
[56] Xiong Cao et al. Band Gap Opening of Graphene by Forming Heterojunctions with the 2D Carbonitrides Nitrogenated Holey Graphene, g‑C3N4, and g‑CN: Electric Field Effect,journal of Physical chemistry c, (2016)
[57] Balu, R.; Zhong, X.; Pandey, R.; Karna, S. P. Effect of Electric Field on the Band Structure of Graphene/Boron Nitride and Boron Nitride/Boron Nitride Bilayers.Appl. Phys. Lett.2012, 100, .052104
[58] Zhong, X.; Yap, Y. K.; Pandey, R.; Karna, S. P. First-Principles Study of Strain-Induced Modulation of Energy Gaps of Graphene/BN and BN Bilayers.Phys. Rev. B: Condens. Matter Mater. Phys.2011, 83,.193403
[59] Du, A.; Sanvito, S.; Li, Z.; Wang, D.; Jiao, Y.; Liao, T.; Sun, Q.;Ng, Y. H.; Zhu, Z.; Amal, R.; et al. Hybrid Graphene and Graphitic Carbon Nitride Nanocomposite:

Gap Opening, Electron-Hole Puddle,Interfacial Charge Transfer, and Enhanced Visible Light Response. J.Am. Chem. Soc.2012, 134, .4397−4393
[60] Li, X.; Dai, Y.; Ma, Y.; Han, S.; Huang, B. Graphene/g-C3N 4Bilayer: Considerable Band Gap Opening and Effective Band Structure Engineering.Phys. Chem. Chem. Phys.2014, 16, 4235−4230
[61] Mahmood, J.; Lee, E. K.; Jung, M.; Shin, D.; Jeon, I. Y.; Jung, S.M.; Choi, H. J.; Seo, J. M.; Bae, S. Y.; Sohn, S. D.; et al. Nitrogenated Holey Two-Dimensional Structures.Nat. Commun.2015, 6, .6486
[62] Mintae Ryu, Paengro Lee, Jingul Kim, Heemin Park and Jinwook Chung , Band gap engineering for single-layer graphene by using slow Li+ions Nanotechnology27(2016) 31LT03(7pp),(2016)
[63] Eizenberg, M., Blakely, J.M.: Carbon monolayer phase con- densation on Ni(111). Surf. Sci. 82(1–2), 228–236 (1979). doi:10.1016/0039-6028(79)90330-3
[64] Eizenberg, M., Blakely, J.M.: Carbon interaction with nickel surfaces: monolayer formation and structural stability. J Chem Phys 71(8), 3467 (1979). doi:10.1063/1.438736
[65] Lang, B.: A LEED study of the deposition of carbon on platinum crystal surfaces. Surface Science 53(1), 317–329 (1975). doi:10. 1016/0039-6028(75)90132-6
[66] Lu, X.K., Yu, M.F., Huang, H., Ruoff, R.S.: Tailoring graphite with the goal of achieving single sheets. Nanotechnology 10(3), 269–272 (1999). doi:10.1088/0957-4484/10/3/308
[67] Zhang, Y.B., Small, J.P., Pontius, W.V., Kim, P.: Fabrication and electric-field dependent transport measurements of meso- scopic graphite devices. Appl. Phys. Lett. 86, 073104 (2005). doi:10.1063/1.1862334
[68] Novoselov, K.S., Geim, A.K., Morozov, S.V., Jiang, D., Zhang, Y., Dubonos, S.V., Grigorieva, I.V., Firsov, A.A.: Electric field effect in atomically thin carbon films. Science 306(5696), 666–669 (2004). doi:10.1126/science.1102896
[69] Novoselov, K.S., Jiang, D., Schedin, F., Booth, T.J., Khotke- vich, V.V., Morozov, S.V., Geim, A.K.: Two-dimensional atomic crystals. PNAS 102(3), 10451–10453 (2005). doi:10. 1073/pnas.0502848102
[70] Balandin, A.A., Ghosh, S., Bao, W.Z., Calizo, I., Teweldebrhan, D., Miao, F., Lau, C.N.: Superior thermal conductivity of single- layer graphene. Nano. Lett. 8(3), 902–907 (2008). doi:10.1021/ nl0731872
[71] Boehm, H.P., Setton, R., Stumpp, E.: Nomenclature and termi- nology of graphite intercalation compounds (IUPAC Recom- mendations 1994). Pure Appl. Chem. 66(9), 1893–1901 (1994). doi:10.1351/pac199466091893
[72] Novoselov, K.S., Geim, A.K., Morozov, S.V., Jiang, D., Zhang, Y., Dubonos, S.V., Grigorieva, I.V., Firsov, A.A.: Electric field effect in atomically thin carbon films. Science 306(5696), 666–669 (2004). doi:10.1126/science.1102896
[73] Novoselov, K.S., Jiang, D., Schedin, F., Booth, T.J., Khotke- vich, V.V., Morozov, S.V., Geim, A.K.: Two-dimensional atomic crystals. PNAS 102(3), 10451–10453 (2005). doi:10. 1073/pnas.0502848102
[74] Allen, M.J., Tung, V.C., Kaner, R.B.: Honeycomb carbon: a review of graphene. Chem. Rev. 110(1), 132–145 (2010). doi:10.1021/cr900070d
[75] Viculis, L.M., Mack, J.J., Kaner, R.B.: A chemical route to carbon nanoscrolls. Science 299(5611), 1361 (2003). doi:10. 1126/science.1078842
[76] Park, S., Ruoff, R.S.: Chemical methods for the production of graphenes. Nat. Nanotechnol. 4, 217–224 (2009). doi:10.1038/ nnano.2009.58

[77] Reina, A., Jia, X.T., Ho, J., Nezich, D., Son, H., Bulovic, V., Mildred Dresselhaus, S., Kong, J.: Large area, few-layer gra- phene films on arbitrary substrates by chemical vapor deposi- tion. Nano Lett. 9(1), 30–35 (2009). doi:10.1021/nl801827v
[78] Jiao, L.Y., Wang, X.R., Diankov, G., Wang, H.L., Dai, H.J.: Facile synthesis of high-quality graphene nanoribbons. Nat. Nanotechnol. 5(5), 321–325 (2010). doi:10.1038/nnano.2010.54
[79] Kosynkin, D.V., Higginbotham, A.L., Sinitskii, A., Lomeda, J.R., Dimiev, A., Price, B.K., Tour, J.M.: Longitudinal unzip- ping of carbon nanotubes to form graphene nanoribbons. Nature 458(7240), 872–876 (2009). doi:10.1038/nature07872
[80] Jiao, L.Y., Zhang, L., Wang, X.R., Diankov, G., Dai, H.J.: Narrow graphene nanoribbons from carbon nanotubes. Nature 458(7240), 877–880 (2009). doi:10.1038/nature07919
[81] Xin, G. Q., W. Hwang, N. Kim, S. M. Cho, and H. Chae.: A graphene sheet exfoliated with microwave irradiation and interlinked by carbon nanotubes for high-performance trans- parent flexible electrodes. Nanotechnology Vol. 21, No. 40 (2010). 10.1088/0957-4484/21/40/405201
[82] Sutter, P.: Epitaxial graphene: how silicon leaves the scene. Nat. Mater. 8(3), 171–172 (2009). doi:10.1038/nmat2392
[83] Novoselov, KS, *et al.*; *Science* **306**, 666-669,(2004)
[84] Casiraghi C, *et al.*; *Nano Letters* **7**, 2711-2717, (2007)
[85] Y. Xu, H. Bai, G. Lu, C. Li and G. Shi, J. Am. Chem. Soc., 130 (2008) 5856.
[86] S. Stankovich, D.A. Dikin, R.D. Piner, K.A. Kohlhaas, A. Kleinhammes A, Y.Y. Jia, Y. Wu, S.T. Nguyen and R.S. Ruoff, Carbon, 45 (2007) 1558.
[87] S. Park and R.S. Ruoff, Nature Nanotechnol., 4 (2009) 217.
[88] Lotya M, *et al.*; *ACS Nano* **4**, 3155-3162 (2010)
[89] Su CY, *et al.*; *ACS Nano* **5**, 2332-2339 (2011)
[90] Forbeaux I, *et al.*; *Phys. Rev. B* **58**, 16396-16406 (1998)
[91] Cambaz ZG, *et al.*; *Carbon* **46**, 841-849 (2008)
[92] Enderlein, C; Dissertation: Graphene and its Interaction with Di erent Substrates Studied by Angular-Resolved Photoemission Spectroscopy, Freie Universitaet Berlin (2010)
[93] Robertson AW, Warner JH, unpublished (2011)
[94] Kim KS, *et al.*; *Nature* **457**, 706-710 (2009
[95] Bae, S, *et al.*; *Nature Nanotech.* **5**, 574-578 (2010)
[96] Forbeaux, I., Themlin, J. M. & Debever, J. M. Heteroepitaxial graphite on 6H-SiC(0001): interface formation through conduction-band electronic structure. *Phys. Rev. B* 58, 16396–16406 (1998).
[97] Berger, C. *et al.* Ultrathin epitaxial graphite: 2D electron gas properties and a route toward graphene-based nanoelectronics. *J. Phys. Chem. B* 108, 19912–19916 (2004).
[98] Ohta, T., Bostwick, A., Seyller, T., Horn, K. & Rotenberg, E. Controlling the electronic structure of bilayer graphene. *Science* 313, 951–954 (2006).
[99] Virojanadara, C. *et al.* Homogeneous large-area graphene layer growth on 6H-SiC(0001). *Phys. Rev. B* 78, 245403 (2008).
[100] Core-Shell Nanowire Geometry. ACS Nano 2012, 6, 6687−6692.
[101] Tsai, D. S.; Lin, C. A.; Lien, W. C.; Chang, H. C.; Wang, Y. L.;

He, J. H. Ultra-High-Responsivity Broadband Detection of Si MetalSemiconductor-Metal Schottky Photodetectors Improved by ZnO Nanorod Arrays. ACS Nano 2011, 5, 7748−7753.

[102] Hsiao, Y. H.; Chen, C. Y.; Huang, L. C.; Lin, G. J.; Lien, D. H.; Huang, J. J.; He, J. H. Light Extraction Enhancement with Radiation Pattern Shaping of Light Emitting Diodes by Waveguiding Nanorods with Impedance-Matching Tips. Nanoscale 2014, 6, 2624−2628.

[103] Ho, C. H.; Lien, D. H.; Hsiao, Y. H.; Tsai, M. S.; Chang, D.; Lai, K. Y.; Sun, C. C.; He, J. H. Enhanced Light-Extraction from Hierarchical Surfaces Consisting of p-GaN Microdomes and SiO2 Nanorods for GaN-Based Light-Emitting Diodes. Appl. Phys. Lett. 2013, 103, 161104.

[104] Gokus, T. *et al.* Making graphene luminescent by oxygen plasma treatment. *ACS Nano* **3,** 3963–3968 (2009).

[105] Ha, H. D., Jang, M.-H., Liu, F., Cho, Y.-H. & Seo, T. S. Upconversion photoluminescent metal ion sensors via two photon absorption in graphene oxide quantum dots. *Carbon* **81,** 367–375 (2015).